

Global warming impacts on rockfall frequency and magnitude due to changing frost distribution and frost cracking effectiveness

Tom Birien  | Francis Gauthier | Francis Meloche

Centre d'étude nordiques (CEN), Laboratoire de géomorphologie et de gestion des risques en montagne (LGGRM), Université du Québec à Rimouski (UQAR), Rimouski, Quebec, Canada

Correspondence

Tom Birien, Centre d'étude nordiques (CEN), Laboratoire de géomorphologie et de gestion des risques en montagne (LGGRM), Université du Québec à Rimouski (UQAR), Rimouski, Canada.

Email: tom_birien@uqar.ca

Funding information

Ministère des Transports du Québec (MTQ); Natural Sciences and Engineering Research Council of Canada (NSERC)

Abstract

The distribution of freezing and thawing within rock masses is time varying (day to day or season to season) and controls the effectiveness of the frost cracking processes from the surface until various depths. These processes are major contributors to the development of rock instabilities. By altering the thermal regime of rockwalls, global warming could have a major impact on rockfall dynamic by the end of the 21st century. This study seeks to improve our understanding of the influence of this warming on (i) the distribution of freezing and thawing within rock masses, (ii) the effectiveness of frost cracking and (iii) the frequency and magnitude of rockfalls. Thermistor sensors inserted in a 5.5-m horizontal borehole and a weather station were installed on a vertical rockwall located in the northern Gaspé Peninsula (Canada). This instrumentation was used to calculate the surface energy balance of the rockwall and to measure and model its thermal regime at depth over a period of 28 months. Combining locally recorded historical air temperature data with simulated future data (scenarios RCP4.5 and RCP8.5) made it possible to extend the rockwall thermal regime model over the period 1950–2100. The effectiveness of frost cracking over this 150-year period has been quantified using a thermomechanical model. Depending on the scenario, warming of 3.3°C to 6.2°C is expected on the northern Gaspé Peninsula by the end of the 21st century. This rapid warming is likely to decrease the maximum depth reaches by the seasonal frost by 1–2 m and shorten its duration by 1–3 months. The frequency of freeze–thaw cycles could increase twelvefold in January. Frost cracking effectiveness should intensify around 70 cm in depth and disappear beyond that (RCP4.5) or diminish starting at 10 cm in depth (RCP8.5). In areas subject to seasonal freeze–thaw cycles, decimetric rockfall frequency could grow considerably in winter but be significantly reduced in fall and spring. Furthermore, frost cracking would cease contributing to the development of larger magnitude instabilities.

KEYWORDS

freeze–thaw cycle, frost cracking, frost damage, global warming, rockfall

1 | INTRODUCTION

Through perturbation to the precipitation and temperature regimes, climate change has significant impacts on hillslope dynamics and

processes (Crosta & Clague, 2009; Crozier, 2010; Gariano & Guzzetti, 2016; Huggel et al., 2012; Korup et al., 2012; Sidle & Ochiai, 2006). However, how these perturbations interact with the occurrence, frequency and magnitude of slope movements remains

This is an open access article under the terms of the [Creative Commons Attribution](https://creativecommons.org/licenses/by/4.0/) License, which permits use, distribution and reproduction in any medium, provided the original work is properly cited.

© 2024 The Author(s). *Earth Surface Processes and Landforms* published by John Wiley & Sons Ltd.

challenging to understand (Alvioli et al., 2018; Gariano & Guzzetti, 2016; Huggel et al., 2012). The influence of climate change on those movements is a function of the material, type of movement and the initial and new climatic conditions (Crozier, 2010).

Rockfall is a hillslope movement in which blocks of various magnitude detach from the surface of rock escarpments (Budetta, 2004; Michoud et al., 2012; Piteau & Peckover, 1978; Selby, 1993). While spontaneous, rockfalls result from a series of processes that interact over long periods. It never result solely from the latest apparent change (Draebing & Krautblatter, 2019; Gunzburger et al., 2005; Schovanec, 2020). The two principal climatic factors contributing to the development of rock instabilities in hillslope and mountain environments are precipitation and freeze–thaw (FT) cycles (Birien & Gauthier, 2023a; Collins & Stock, 2016; Coutard & Francou, 1989; D'Amato et al., 2016; Delonca et al., 2014; Hungr et al., 1999; Matsuoka & Sakai, 1999; Rapp, 1960; Wieczorek & Jäger, 1996). While the influence of climate change on precipitation regimes is highly variable on the global scale, rising air temperatures affect the entire planet and are particularly significant at high latitudes and elevations (Collins et al., 2013; Hartmann et al., 2013). Global warming alters the distribution of freezing and thawing within rock masses and, by extension, the effectiveness of the main frost cracking processes (Rode et al., 2016). Frost cracking is defined as the breakdown of rocks by freezing (Walder & Hallet, 1985), and two main processes can conduct to frost cracking: the volumetric expansion of freezing water and ice segregation (Matsuoka & Murton, 2008; Rode et al., 2016). Frost damage induced by the volumetric expansion of freezing water requires a temperature below the freezing point and a rock water saturation of over 90% (Walder & Hallet, 1986), and frost damage due to ice segregation within the rock requires colder 'frost cracking windows' (Anderson, 1998) that depend on rock strength (Mayer, Deprez, et al., 2023a; Walder & Hallet, 1985). Hallet et al. (1991) have shown that the most efficient temperature range was between -6°C and -3°C for low-strength rock, and Walder & Hallet (1985) have obtained values between -15°C and -4°C for high-strength rocks. Mayer, Deprez, et al. (2023a) have recently suggested that initial rock moisture content is not a primary control of ice segregation, and Mayer, Eppes, & Draebing (2023b) have shown that ice segregation occurs on low-saturated (30%) samples. Modern climate warming should have repercussions on the effectiveness of volumetric expansion and on ice segregation processes, and these repercussions are already apparent in the frequency of rockfalls of varying magnitudes in alpine periglacial environments (Gobiet et al., 2014; Gruber et al., 2004; Gruber & Haeberli, 2007; Harris et al., 2009; Hartmeyer et al., 2020; Huggel, 2009; Huggel et al., 2012; Paranunzio et al., 2016; Ravel & Deline, 2011).

Modern climate warming is only in its infancy (Collins et al., 2013; Hartmann et al., 2013), and the already considerable impact of global warming on rockfall dynamics (Hartmeyer et al., 2020; Ravel & Deline, 2011a) can make human populations and infrastructure more vulnerable (Haque et al., 2019; Mourey et al., 2020; Mourey et al., 2022; Pröbstl-Haider et al., 2021). The intensification of climate warming expected over the coming decades (Collins et al., 2013; Hartmann et al., 2013) raises a number of questions. To what extent will climate warming in the 21st century alter the distribution of freezing and thawing within rock? What repercussions on the effectiveness of frost cracking can be expected? What will be the impact on rockfall frequency and magnitude?

Most studies on the impacts of climate warming on rockfall dynamic between the present and the end of the 21st century are qualitative and hypothetical in nature (Gruber et al., 2004; Huggel, 2009; Ravel & Deline, 2011). The development of some models that allow to calculate the surface and near-surface temperature of rock slopes using meteorological data as input can be used to quantify the effects of future global warming on rock slopes affected by permafrost or dominated by seasonal frost (SF) or sporadic FT cycles (on the scale of few hours to few days). Hales & Roering (2007) have modelled high mountain permafrost distribution 100 and 200 years in the future and assume surface warming of $2.5\text{--}3.5^{\circ}\text{C}$, depending on slope aspect. They have shown that even if permafrost degradation could occur in few decades near the rock mass surface, relict permafrost could persist at greater depth for centuries. In the French Alps, Magnin et al. (2017) modelled the long-term evolution of permafrost in three vertical cross sections of rockwall sites with elevation ranging between 3160 and 4300 m from the Little Ice Age to 2100. They have shown that the rate of change between 1850 and the early 1990s was in the same range as the one experienced during the past three decades. By the end of the 21st century, even the core of wide summits will be strongly affected by the global warming (Magnin et al., 2017). Rode et al. (2016) compared periods favourable to frost cracking in the Austrian Alps in 2010 and 2100. They have shown that by the end of the 21st century, such periods can be expected to dwindle at low elevations. In contrast, in high elevation permafrost zone, these periods are likely to be longer due to more frequent thaw periods and a higher availability of liquid water (Rode et al., 2016). Studies by Hales & Roering (2007), Magnin et al. (2017) and Rode et al. (2016) illustrate how the modern global warming is affecting the frost distribution in rock masses, but their aim was neither to quantify the evolution of the effectiveness of frost cracking nor to discuss the evolution of the frequency and magnitude of rock instabilities within the larger context of modern climate change. Several methods developed in the last decades allow to model the frost cracking process (Anderson, 1998; Hales & Roering, 2007; Rempel et al., 2016; Walder & Hallet, 1985). Two are purely thermal models (Hales & Roering, 2007; Anderson, 1998), and models developed by Walder and Hallet (Walder & Hallet, 1985) and by Rempel et al. (2016) are thermomechanical models. The thermomechanical model of Rempel et al. (2016) is based on the model developed by Walder & Hallet (1985) and assumes that frost damage is correlated with porosity increases under conditions where frost cracking takes place. They make the assumption that porosity increases driven by the formation of ice lenses occurs parallel to the frost cracking front (Rempel et al., 2016). Hydraulic, thermal and mechanical properties of rock masses controlled the frost cracking effectiveness, but these properties are difficult to measure, especially at a landscape scale (Draebing & Mayer, 2021). Nevertheless, even if inherent limitations in model combinations or availability of input data (e.g. rock water content) could remain challenging, these tools could be greatly relevant to model the evolution of the efficiency of frost cracking by the end of the 21st century.

The main objectives of this study are to analyse the influence of global warming on (1) the evolution of the freezing and thawing distribution within the rockwall, (2) the evolution of frost damage over time and at different depths and (3) the frequency and magnitude of rock instabilities in environments subject to FT cycles. To achieve those

objectives, we modelled the thermal regime of a rockwall on the northern Gaspé Peninsula (Canada) using a dataset composed of air temperature data collected from 1950 to present along and simulated data from present to 2100. On the basis of this 150-year air temperature time series, we modelled the evolution of frost cracking effectiveness using the model designed by Rempel et al. (2016).

2 | STUDY AREA

This study was carried in northern Gaspésie (Figure 1). The local relief is dominated by glacial valleys (Héту & Gray, 1985) that separate rocky plateaus reaching 400–600 m in elevation. The junction between these plateaus and the Gulf of St. Lawrence is marked by rock walls. Cut into Ordovician flysch, these rockwalls are mainly composed of alternating strata of sandstone, greywacke, siltstone and pelagic shale of multi-decimetre thickness (Enos, 1969a, 1969b). These rocks are highly fissile and promote a high density of rock discontinuities (Héту & Vandelac, 1989). They show a high retreat rate ($3 \text{ mm}\cdot\text{a}^{-1}$) and high frequency of rockfall (1 per $13 \text{ m}^2\cdot\text{a}^{-1}$) (Birien & Gauthier, 2023a). Most rock slopes are facing north, which limits the influence of solar radiation on rock temperature. They are in constant shade from mid-October to mid-March and become exposed again to the late afternoon sun in spring. Most of them are steep ($70\text{--}90^\circ$) and not conducive to snow accumulation (Birien & Gauthier, 2023a). The area is characterized by a humid continental climate with short cool summers, according to the Köppen climate classification system (Beck et al., 2018). Weather data for the period 1991–2020 from Cap-Madeleine weather station ($49^\circ 15' 03'' \text{N } 65^\circ 19' 29'' \text{W}$) (Figure 1) show that it has an annual mean temperature of 3.9°C and warmest (July) and coldest (January) month mean temperatures of 16.3°C and -9.2°C , respectively. Over this 30-year period, it received a total

annual precipitation of 888 mm, 33% of which fell as snow (Environnement Canada, 2021).

3 | METHODOLOGY AND METHODS

A time series of air temperatures from 1 January 1950 to 31 December 2099 was constructed using locally recorded historical data (1950–2020) and simulated data (2021–2099). This time series was then used to model the thermal regime of a rockwall, which was previously validated with temperatures measured up to 5.5 m in depth between 10 June 2018 and 8 October 2020 (Site MAE, Figure 1). Based on this thermal regime model, the evolution of the FT characteristics and the frost cracking intensity within the rockwall were analysed and compared for typical 30-year climatic normal periods: 1950–1979, 1980–2009, 2010–2039, 2040–2069 and 2070–2099 (Figure 2).

3.1 | Air temperature datasets

Historical data (1950–2020) come from hourly air temperature collected at the Environment Canada weather station at Cap-Madeleine (Figure 1). Weather data from this station are continuous during this period, except for a few gaps of 1–7 days, which have been filled using data from another Environment Canada weather station at Cap-Chat, located 95 km to the west.

Five simulated daily air temperature time series (1970–2100) were extracted from three Regional Climate Models (RCMs) driven by three Coupled Global Climate Models (GCMs) (Table 1). These five simulations, characterized by a 0.44° grid mesh (around a 50-km grid resolution), were obtained from the North America Coordinated

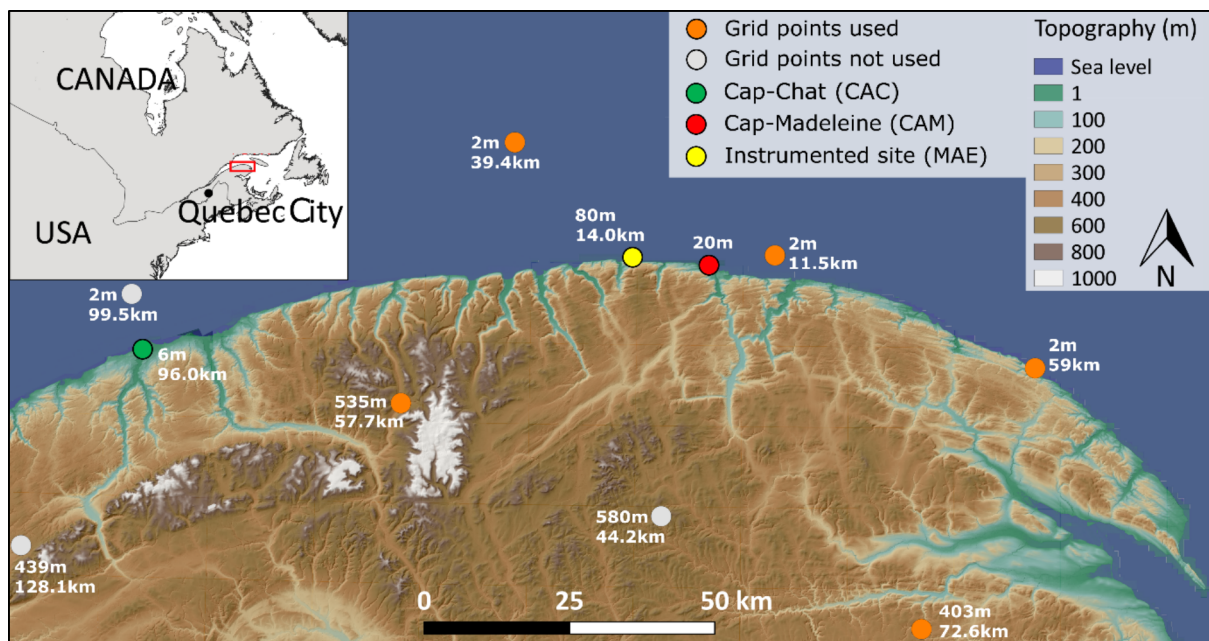


FIGURE 1 Location map showing the Environment Canada weather stations at Cap-Chat (green dot, $49^\circ 06' 33'' \text{N } 66^\circ 39' 16'' \text{W}$) and at Cap-Madeleine (red dot, $49^\circ 15' 03'' \text{N } 65^\circ 19' 29'' \text{W}$), the instrumented rockwall with weather station and temperature logger (yellow dot, $49^\circ 15' 14'' \text{N } 65^\circ 31' 38'' \text{W}$) and the NAM-44 grid points (orange dots) used for climate projection. Elevation is given for each grid point, like the distance between these points and the weather station of Cap-Madeleine.

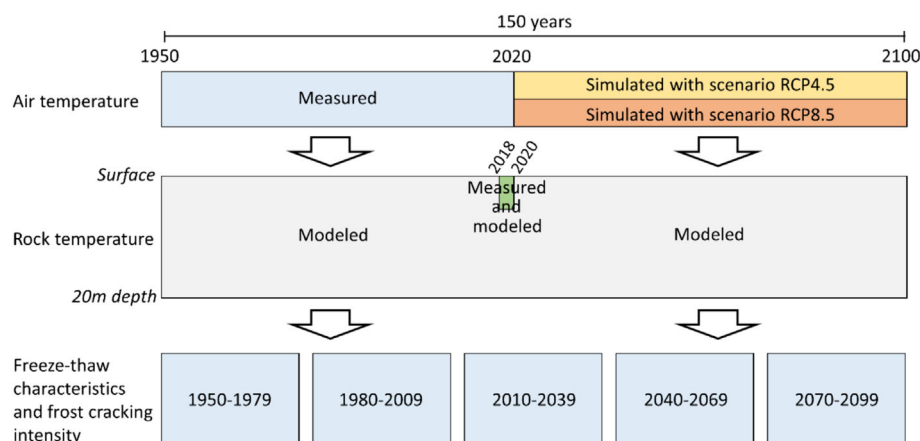


FIGURE 2 Summary of methodological steps used to analyse the influence of global warming on Rockwall thermal regime and frost cracking.

TABLE 1 The five simulations used in this study from Regional Climate Models (RCMs) driven by different Coupled Global Climate Models (GCMs). The simulations used two Representative Concentration Pathways (RCP4.5 and RCP8.5). This North American climate data were obtained from the NA-CORDEX database (Mearns et al., 2017).

Regional Climate Models	Driven conditions from coupled global climate	Institutions for cGCMs
HIRHAM (Christensen et al., 2007)	ICHEC-EC-EARTH	Irish Centre for High End Computing (ICHEC), Ireland
CRCM5 (Martynov et al., 2013; Šeparović et al., 2013; Zadra et al., 2008)	CCCma-CanESM2 MPI-M-MPI-ESM	Canadian Centre for Climate Modelling and Analysis (CCCma), Canada Max Planck Institut (MPI), Germany
RCA4 (Samuelsson et al., 2011)	CCCma-CanESM2 ICHec-EC-EARTH	Canadian Centre for Climate Modelling and Analysis (CCCma), Canada Irish Centre for High and Computing (ICHEC), Ireland

Regional Climate Downscaling Experiment (CORDEX-NA) project (Mearns et al., 2017). The simulations were done under moderate (RCP4.5) and high (RCP8.5) Representative Concentration Pathways (RCPs). We selected RCP4.5 and RCP8.5 as they represent middle- and worst-case climate change scenarios (van Vuuren et al., 2011). The five simulations have been chosen because their basic states are very close to the observational records of the 1970-1999 historical period.

The 50-km resolution of the GCMs data needs to be downscaled for a better representativity of the temperature measured at the weather station (CAM). To support the grid point selection, simulated temperatures from the GCMs have been compared with the historical time series from the CAM weather station (1970-1999). A combination of five grid points has been chosen (Figure 1) according to the goodness-of-fit of the simulated mean temperature (from the five GCMs) on the measured temperature during this historical period (coefficient of determination). The grid points selection has also been guided by their respective distances from CAM, their elevation and

their geographical location (maritime and continental influence). The models output included the minimum, mean and maximum daily temperatures. With the use of linear interpolation between the minimum and maximum daily temperatures, we extracted hourly data for the future period to match the time scale of the historical period as well as the time scale of the software we used to model rock temperature (WUFI® Pro). Finally, historical data were combined with climate projection data to obtain a 150-year time series (1950-2100). At this point, the temperatures simulated with the five models were not averaged to avoid loss of information on climate extremes.

3.2 | Meteorological and rockwall temperature datasets

A small weather station was installed in June 2018 at 20 m from the top of a 100 m high vertical rockwall facing north (MAE) located 15 km west of Cap-Madeleine weather station (Figure 1). The weather station measures air temperature, incident and reflected solar radiation perpendicular to the rockwall and wind speed and direction (Figure 3). Atmospheric pressure and incident and reflected long wavelength radiation were recorded from another weather station located on the scree slope under the rockwall (Table 2). The rockwall temperature was measured with a thermistor string inserted into a borehole perpendicular to the surface. The 2-inch diameter borehole was carried out with a drill (Figure 3) connected to an air compressor at the top of the rockwall. Thermistors were installed at depths of 0.01 (near surface), 0.3, 0.6, 1.0, 1.5, 2.0, 2.5, 3.0, 3.5, 4.0, 4.5, 5.0 and 5.5 m. A continuous temperature profile of rock was produced using linear interpolation between the thermistors. The purpose of this instrumentation was to (1) calculate the energy balance at the rockwall surface and (2) measure its thermal regime up to 5.5 m in depth. The data collection period covered 28 months from 10 June 2018 to 8 October 2020. Readings were taken every 15 min and averaged to get hourly data.

3.3 | Rock temperature and frost damage modelling

Modelling surface thermal signal propagation to depth requires detailed knowledge of site lithology. Several intact sample blocks

FIGURE 3 Instrumented rockwall (MAE) including 20-m-long chain link protective fences (1), wind direction sensor (2), wind speed sensor (3), pyranometers (4), air temperature sensor (5), datalogger (6), rock temperature thermistances up to 5.5 m deep (7) and back-up rock temperature thermistances up to 0.5 m deep (8). Our drill set-up is pictured on the lower left-hand corner.



TABLE 2 Instruments used to (i) assess the energy balance at the rockwall surface and (ii) measure its thermal regime from the surface to 5.5 m in depth.

Data	Unit	Instrument (company)	Accuracy
Air temperature	°C	Air temperature sensor TMC6-HD + Solar radiation shield M-RSA (HOBO by Onset)	±0.25°C
Rock temperature	°C	Thermistor string 915 MHz + minilogger M-Log5WDALLAS-US (Geoprecision)	±0.25°C
Incident solar radiation Reflected solar radiation	W/m ²	Pyranometer S-LIB-M003 (HOBO by Onset)	±10 W/m ²
Incident infrared radiation Reflected infrared radiation	W/m ²	Pyrgometer SN-500-SS (Apogee Instruments)	±8.5 W/m ²
Wind and gust speed Wind direction	m/s ∅	Wind speed and direction sensor S-WSET-B (Onset)	±1.1 m/s ±5°
Air pressure	mbar	Barometric pressure sensor S-BPB-CM50 (Onset)	±5.0 mbar

about 20 cm long were collected directly from the rockwall surface: 7 blocks of greywacke, 9 blocks of siltstone and 3 blocks of shale. Natural discontinuities in the rock masses, particularly in the stratified siltstone and shale blocks, made it possible to separate the samples without weakening them. At the Laboratoire de géomorphologie et de gestion des risques en montagne (LGGRM), the volume, dry mass and water saturated mass of each sample were measured to calculate their density and porosity (ISRM, 1979). All the samples have been dried in an oven for 1 week and weighed before being immersed in water during one additional week or until their weight have stabilized. The thermal properties of the samples were measured at the Laboratoire ouvert de géothermie (LOG) at the Institut National de la Recherche Scientifique Eau Terre Environnement Research Centre (INRS-ETE). The LGM Lippmann TCSCAN infrared scanner was used to measure the thermal conductivity and diffusivity of each sample (Lippmann and Rauén GbR, 2022). Because siltstone and shale are anisotropic rocks, thermal signals that are perpendicular or parallel to the bedding plane do not propagate at the same speed. For 2D anisotropic rock samples, the average thermal conductivity and diffusivity values are calculated using the method developed by Popov et al. (2016). This method

allows to derive the conductivity parallel and perpendicular to the layering plane from only 2 scan lines per sample (Popov et al., 2016). Thermal capacity of each sample was then calculated from the thermal density, conductivity and diffusivity values. In this way, average values of the thermal parameters for each type of rock were calculated from collection of samples.

WUFI® Pro is an easy-to-use, menu-driven program designed to model transient one-dimensional heat and moisture transfer (Karagiozis et al., 2001). It is usually used to assess the hygrothermal behaviour of a wide range of building material classes under climatic conditions (Karagiozis et al., 2001), but it has also previously been used to successfully model the thermal regime and moisture of rock masses (Rode et al., 2016; Sass, 2005; Schnepfleitner et al., 2018). The model is adapted for cold climate because it considers parameters like freeze–thawing mechanism or latent heat of phase change conditions (Karagiozis et al., 2001). All the weather conditions measured at the rockwall surface and detailed into the Table 2 served as inputs into the software to model the rock surface temperature along the time (hourly between 10 June 2018 and 8 October 2020). Slope, topographical aspect, heat-transmission resistance and short-

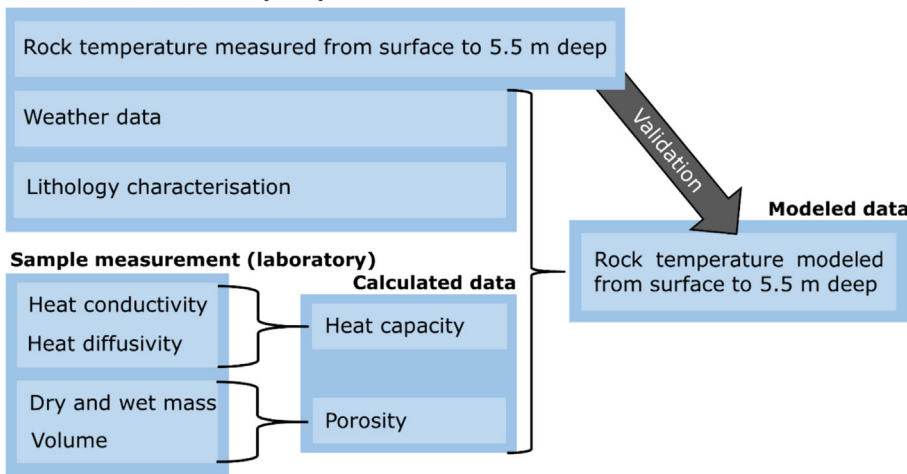
Rockwall measurement (field)

FIGURE 4 Data obtained from our field and laboratory measurements to model rock temperature in WUFI® Pro.

wavelength radiation absorption are commonly used parameters into the software to model the rock surface temperature. These parameters were not required in our case because the weather station measures incident and reflected solar radiation perpendicular to the rockwall as well as wind speed and direction directly on the rockwall (Figure 3). The coefficient of determination is the statistic test used to validate the surface temperature time series modelled from the measurements recorded directly at the rockwall surface.

To assess the influence of this surface temperature into the rockwall thermal regime, physical properties (density, porosity) and rock thermal properties (conductivity, capacity and diffusivity) measured have been added as input in WUFI® Pro. The propagation of the modelled thermal signal was validated using measured data (coefficient of determination) by modulating the thickness and nature (thermal properties) of the rock layers traversed. That combination of thickness and nature had to correspond to the geological units observed on the rockwall surfaces (Figure 3). Figure 4 summarizes the protocol used in this study. Although our instrumentation limited the temperature measurements to 5.5 m in depth, we modelled them to a depth of 20 m. The mesh width of the numerical grid has been defined to 1 cm for all the 20-m profile. Model the water saturation degree was not the aim of this study but because the thermal properties of rocks are dependant of this water saturation degree (Albert et al., 2017), a value has to be set. In the Alps, Sass (2005) modelled the degree of saturation in a rockwall that stabilized around 80% in the first decimetres below the surface. In the absence of local measurements, this average value was used at the surface, and we assume that this value is constant on the entire modelled profile.

After the model was validated with the rockwall temperature measured between 1 June 2018 and 8 October 2020, it has been used to simulate the thermal regime between 1 January 1950 to 31 December 2099. The time series of air temperatures, constructed from historical and simulated data (Figure 2), was used as input in the model. As modelled by Lachenbruch et al. (1988), the year-to-year variability of surface temperatures become negligible in rockslope at the depth of 20 m, and this constant temperature is equal to the mean annual air temperature. Nevertheless, in a climate change context, the temperature can evolve at greater depths (Lachenbruch et al., 1988). Thus, a 30-year moving average of air temperature was used to set

the temperature at 20 m in depth. For example, the 20-m-deep input temperature in 2050 is the mean annual air temperature of the 2020–2049 period. Further studies should help to improve our ability to forecast the evolution of wavelength radiation, atmospheric pressure and wind speed and direction in the current climate change context (Collins et al., 2013; Hartmann et al., 2013). Furthermore, because the instrumented rockwall has a northerly exposure and remains in shadows from mid-October to mid-March, it is mostly affected by air temperature fluctuations in winter (Biriën & Gauthier, 2023b; Gauthier et al., 2013; Gauthier et al., 2015). The values for short and long wavelength radiation, atmospheric pressure and wind speed and direction for the year 2019 were assumed to be representative and looped for each year of the covered period.

In order to quantify the global warming influence on the effectiveness of frost cracking, the thermomechanical model developed by Rempel et al. (2016) was used. The key assumption made by the author is that the increase of porosity is driven by the formation of ice lenses parallel to the frost cracking front (Rempel et al., 2016). Under conditions where frost cracking takes place, their model measures the porosity change in a rock slope, integrated over time, yielding a porosity change profile that should be correlated with frost-driven rock damage. In our study, we used the 150-year period of thermal regime simulated to drive this thermomechanical model. The key parameter of this model is the cracking pressure P_c that determine the upper temperature limit at which frost damage can occur, called the undercooling crack temperature ΔT_c :

$$P_c = \frac{\sqrt{\pi}}{2} \frac{F_t}{\sqrt{x_i}}, \text{ and} \quad (1)$$

$$\Delta T_c \approx \frac{T_m P_c}{\rho_i L}, \quad (2)$$

where T_m is the melt temperature, ρ_i the ice density, L the latent heat, x_i the crack radius and F_t the fracture toughness. The frost damage $\Delta n(z)$ is then defined by the porosity change Δn over depth z . $\Delta n(z)$ represents the frost damage occurring when the temperature melt variation $\Delta T = T_m - T(z, t)$ reached the threshold for the undercooling cracking temperature ΔT_c , integrated over the time period of the temperature series:

TABLE 3 Parameters and values used to feed the thermomechanical model developed by Rempel et al. (2016).

Parameter	Abbreviation	Value	Unit
Ice density	ρ_i	920	Kg m ⁻³
Latent heat	L	334	kJ kg ⁻¹
Bulk melt temperature	T_m	0	°C
Water viscosity	μ	1.8	MPa s
Cracking pressure	P_c	5.03	MPa
Unfrozen permeability	k_0	10 ⁻¹⁶	m ²
Permeability at ΔT_c	k_c	2.5 × 10 ⁻²³	m ²
Power-law exponent	α	4	-
Undercooling for cracking	ΔT_c	4.47	°C
Undercooling for ice formation	ΔT_f	0.1	°C
Crack radius	x_i	0.05	m
Fracture toughness	F_t	0.345	MPa m ^{-1/2}

$$\Delta n(z) = \left(\frac{D}{\Delta T_c^2} \right) \int_{\Delta T > \Delta T_c} \left(\frac{\Delta T_c}{\Delta T} \right)^{\alpha+1} \left(\frac{dT}{dz} \right) dt, \quad (3)$$

where α is an empirical power law exponent (Andersland & Ladanyi, 2003) set at 4 as recommended by Rempel et al. (2016). The diffusivity (D) is defined by $D = \alpha \rho_i L k_c T_c / (T_m \mu)$ in which k_c is the permeability and μ the water viscosity at T_c . All parameter values are presented in Table 3. Except for rock temperatures, fracture toughness and initial crack radius, all other parameters are set according to the study of Rempel et al. (2016). The values of dt and dz were, respectively, set to 0.01 days and 0.01 m to ensure a proper numerical approximation of the derivative while retaining a low computational cost. The initial crack radius was set to 0.05 m (value based on Draebing and Mayer, 2021b; Walder & Hallet, 1985; and Atkinson & Rawlings, 1981). We used a critical F_t value of 0.345 MPa m^{-1/2} as measured by Dwivedi et al. (2000) on a sandstone sample at 0°C with a porosity similar to that measured on the greywacke samples collected in the field. To simplify our analysis, we have chosen to use a constant value of F_t , even if its value should normally decrease over time, especially over such long analysis periods. The decrease in fracture toughness caused by the increasing porosity leads to the detachment of blocks from the rock face and eventually to rockfalls (Gauthier, Birien, & Meloche, 2022a; Gauthier, Laliberté, et al., 2022b). This dynamic of erosion and renewal of rocks directly exposed to the atmosphere has not been considered in the modelling. Thus, the values of porosity change over time should be seen as a proxy of potential rock damage caused by freezing. For further information on the model, please refer to Rempel et al. (2016).

3.4 | Trend analyses

We analysed the seasonal evolution of freezing and thawing distribution within the rockwall and the effectiveness of frost damage over typical 30-year climatic periods: 1950–1979, 1980–2009, 2010–2039, 2040–2069 and 2070–2099. On the basis of those periods, we quantified the impact of climate warming on five parameters used as indicator of the intensity of cryogenic processes:

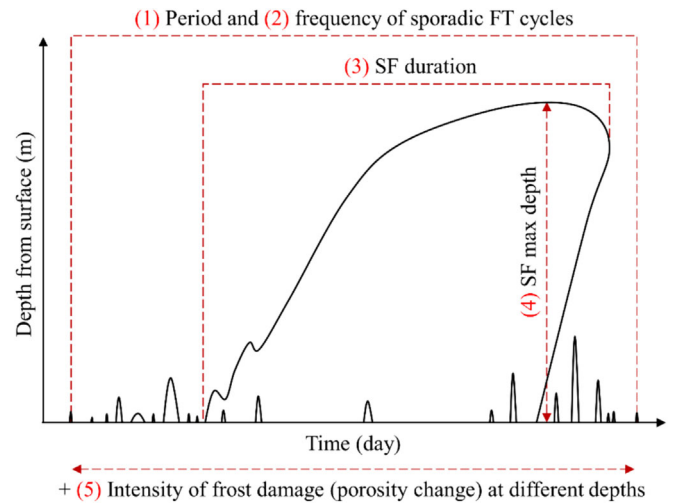


FIGURE 5 Diagram showing thermal parameters quantified for the five climatic periods. Continuous black lines represent occurrences of 0°C.

1. the duration between the earliest autumnal and the last spring FT cycle during a season (Figure 5).
2. the frequency of sporadic FT cycles between the earliest autumnal and the last spring FT cycle each season. Sporadic FT cycle is defined as any cycle, irrespective of duration, that reaches a minimum depth of 0.1 m (Figure 5).
3. the duration and
4. the maximum depth of SF. The SF is defined as the longest uninterrupted period of rockwall temperatures below the freezing point over a winter season. It is the only FT cycle that is not considered as a sporadic cycle during a season (Figure 5).
5. the intensity of frost damage (porosity change) at all depths affected by freezing temperatures into the rockwall (Figure 5).

By definition and as a rule, a threshold temperature of 0°C is considered as the freezing temperature of water in rock masses in different morphoclimatic environments (Coutard & Francou, 1989; D'Amato et al., 2016; Fahey & Lefebure, 1988; Gruber et al., 2004; Hales & Roering, 2007; Kromer et al., 2018). To maintain consistency with those studies, we used 0°C for counting sporadic FT cycles and quantifying the depth and duration of SF.

Averaging the air temperatures produced by the five models (Table 1) attenuates climate extremes and prevents meaningful quantification of the target parameters (Figure 5). To address this issue, rockwall thermal regime was simulated separately for each GCMs. The target parameters were then counted (e.g. frequency of sporadic FT cycles) or quantified (e.g. maximum depth of SF) for each simulation. Finally, an average of those parameters from all simulations was calculated. These same steps were carried out for RCP4.5 and RCP8.5 scenarios.

4 | RESULTS

4.1 | Rock physical and thermal properties

Surrounding to the borehole, where the thermal regime of the rockwall is measured and modelled, the shale strata are on the order

TABLE 4 Bulk density, porosity and thermal parameters measured in the laboratory for the three main types of rock characteristics of our study sites. Values of thermal parameters are for 80% water saturation.

Rock type	Bulk density (kg/m ³)	Porosity (%)	Thermal conductivity (W/mK)	Thermal diffusivity (m ² /s)	Thermal capacity (J/kgK)
Shale	2467	11.32	1.76	5.89e ⁻⁰⁷	1379.24
Siltstone	2987	4.50	3.14	1.24e ⁻⁰⁶	895.04
Graywacke	2574	3.88	3.93	1.58e ⁻⁰⁶	980.06

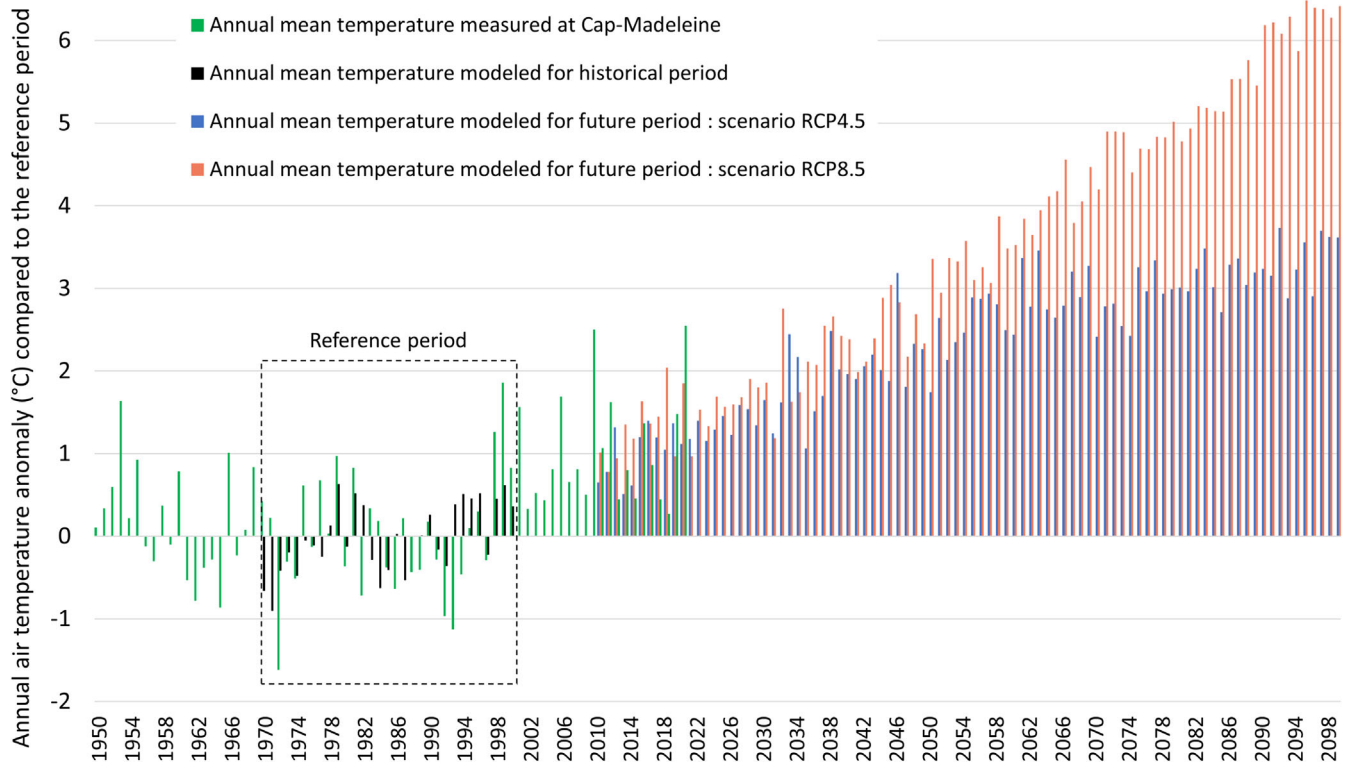


FIGURE 6 Mean annual air temperature anomalies measured at the weather station of Cap-Madeleine (green) and modelled (black) during the reference period and between 2010 and 2100 with scenario RCP4.5 (blue) and RCP8.5 (orange). The mean temperature of the reference period (1970–1999) is 3.3°C.

of centimetres in thickness, and the siltstone and greywacke strata thickness are more variable (decimetre to metre). The density, porosity, thermal conductivity, diffusivity and thermal capacity values measured in laboratory from the study site samples are detailed in Table 4. The proportions of greywacke, siltstone and shale used as input in the 20-m-deep rockwall modelled give average values of thermal conductivity, diffusivity and capacity of 3.52 W m⁻¹ K⁻¹, 1.41e⁻⁰⁶ m²/s and 964.12 J kg⁻¹ K⁻¹, respectively.

4.2 | 1950–2100 air temperature trends

For the historical period used to downscale the modelled temperatures from the GCMs (1970–1999), the mean annual air temperature modelled was equal to 3.28°C, and the value measured at Cap-Madeleine during this same period was equal to 3.30°C (Figure 6). Nevertheless, because they are averaged over five grid points of five simulations, the modelled data show less year-to-year variability than the Cap-Madeleine data (Figure 6).

On the northern Gaspé Peninsula, the measured annual mean air temperature was 3.42°C for the period 1950–1979, compared with 6.41°C modelled according to RCP4.5 and 8.72°C modelled according

to RCP8.5 for the period 2070–2099 (Table 5). Over the 21st century, air temperature can be expected to rise on average by 0.33°C per decade considering RCP4.5 (+3.3°C) and by 0.62°C per decade considering RCP8.5 (+6.2°C). Climate warming should be more pronounced in winter (+0.4°C per decade with RCP4.5, +0.8°C with RCP8.5) than in summer (+0.2°C per decade with RCP4.5, +0.4°C with RCP8.5). Following the RCP8.5, the mean winter temperature should rise above the freezing point (+0.33°C) by the end of the 21st century.

4.3 | Rockwall contemporary thermal regime

From 10 June 2018 to 8 October 2020, the modelled thermal regime is consistent with the measurements recorded in the rockwall (Figure 7). The coefficient of determination of the surface temperature is very high ($R^2 = 0.986$) and rises further with depth ($R^2 = 0.996$ at 0.3 m) as temperature variability decreases. The thermal regime measurements show that the annual temperature amplitude in the rock decreases rapidly with depth (Figure 7): 45°C at the surface, 34°C at 0.3 m, 22°C at 1.0 m and only 6°C at 5.5 m. Modelled amplitude is similar to measured amplitude.

TABLE 5 Mean air temperature for the five consecutive 30-year periods from 1950 to 2100 for two Representative Concentration Pathways (RCP4.5 and RCP8.5).

Period	Mean temperature (°C)		Data source
1950-1979	3.42		Temperature measured (Cap-Madeleine)
1980-2009	3.55		Temperature measured (Cap-Madeleine)
2010-2039	4.73	4.91	Temperature measured until 2020 (Cap-Madeleine) and modeled from 2021
2040-2069	5.85	6.58	Temperature modeled
2070-2099	6.41	8.72	Temperature modeled

The spatio-temporal distribution of freezing and thawing in the rockwall is similar between the measured and the modelled data (Figure 7). In winter 2018–2019, the period of occurrence of FT cycles was 4 days longer with modelled data (194 days) than with the measured data (190 days). The modelled SF was 6 days shorter (127 days), and its maximal depth into the rock mass was lower by 7 cm (4.04 m). In winter 2019–2020, the modelled period of occurrence of FT cycles was identical in duration to the measured period (173 days), the modelled SF was 2 days shorter (141 days) and the modelled maximum depth of SF was greater by 7 cm (3.60 m). During the winter 2019–2020, the number of measured and modelled FT cycles reaching the surface (36 vs 34), 0.1-m depth (23 vs 21) and 0.5-m depth (7 vs 5) were also similar (Figure 7). Because the surface thermistor was over isolated with insulating foam during the previous winter (by mistake), less sporadic FT cycles were probably recorded than it really occurred during the winter 2018–2019. At the onset of these winters (2019, 2020), major surface thaws have resulted in a brief interruption in the freezing front in depth. Most sporadic FT cycles occurred in April (Figure 7) as the intensity of solar radiation rose.

4.4 | FT indicator trends

Results show that modern climate change can be expected to have a significant influence on the duration and the maximum depth of SF. According to RCP4.5, the duration of SF would decrease by 47 days between the periods of 1950–1979 (148 days) and 2070–2099 (101 days). According to RCP8.5, the SF would only persist for 39 days in the period 2070–2099 (Figure 8). The maximum depth of SF would decrease from 4.10 m in the period 1950–1979 to 3.13 m in 2010–2039 and 2.13 m in 2070–2099 considering RCP4.5. The drop is more pronounced considering RCP8.5: the SF would reach a depth of 3.01 m during the period 2010–2039 and just 1.05 m in 2070–2099 (Figure 8).

It is expected that global warming will be accompanied by a change in the period of occurrence of sporadic FT cycles. For the period 1950–

1979, those cycles were concentrated in fall (7.3 in November) and spring (8.2 in April), whereas they were rare in winter (0.5 in January and 0.8 in February) (Figure 9). By the end of the 21st century, winter can be expected to become the period with the highest number of sporadic FT cycles. They could become 2.4, 4.8, 2.9 and 1.5 times more frequent in December, January, February and March, respectively, according to RCP4.5 (Figure 9a) and 2.2, 12.1, 7.7 and 2.0 times more frequent according to RCP8.5 (Figure 9b). Conversely, the previously highly eventful months of November and April can be expected to become periods with a low occurrence of sporadic FT cycles. Their frequency could be divided by 3 in November and by 1.6 in April considering RCP4.5 (Figure 9a). According to RCP8.5, they should become 11.8 and 4.6 less frequent in November and April, respectively (Figure 9a). The disappearance of October and May sporadic FT cycles in the late 21st century is indicative of a shorter freezing period.

Between 1950 and 2099, an inverse relationship can be observed between the normalized frequency of sporadic FT cycles and the maximum depth of SF (Figure 10a). In general terms, as the climate warms, the maximum depth of SF is expected to decrease (Figure 10b), and the frequency of sporadic FT cycles is expected to increase (Figure 10c). During the 150-year study period, the maximum depth of SF is expected to decrease from 4.15 to 2.13 m according to RCP4.5 and from 4.15 to 1.05 m according to RCP8.5 (Figure 10b). The frequency of sporadic FT cycles did not increase between the periods 1950–1979 and 1980–2009; in fact, it decreased slightly (0.14 vs 0.13 FT cycles d^{-1}). In contrast, between the periods 1980–2009 and 2070–2099, this frequency increase by 1.3 considering RCP4.5 and by 1.7 considering RCP8.5 (Figure 10c). Global warming also appears to result in a lower FT cycle frequency at greater depth (Figure 10c).

4.5 | Frost damage indicator trends

For the periods 1950–1979 and 1980–2009, increased porosity caused by the formation of segregated ice could have an impact on the rock to a depth of 3.5 m. The formation of ice lenses could cause

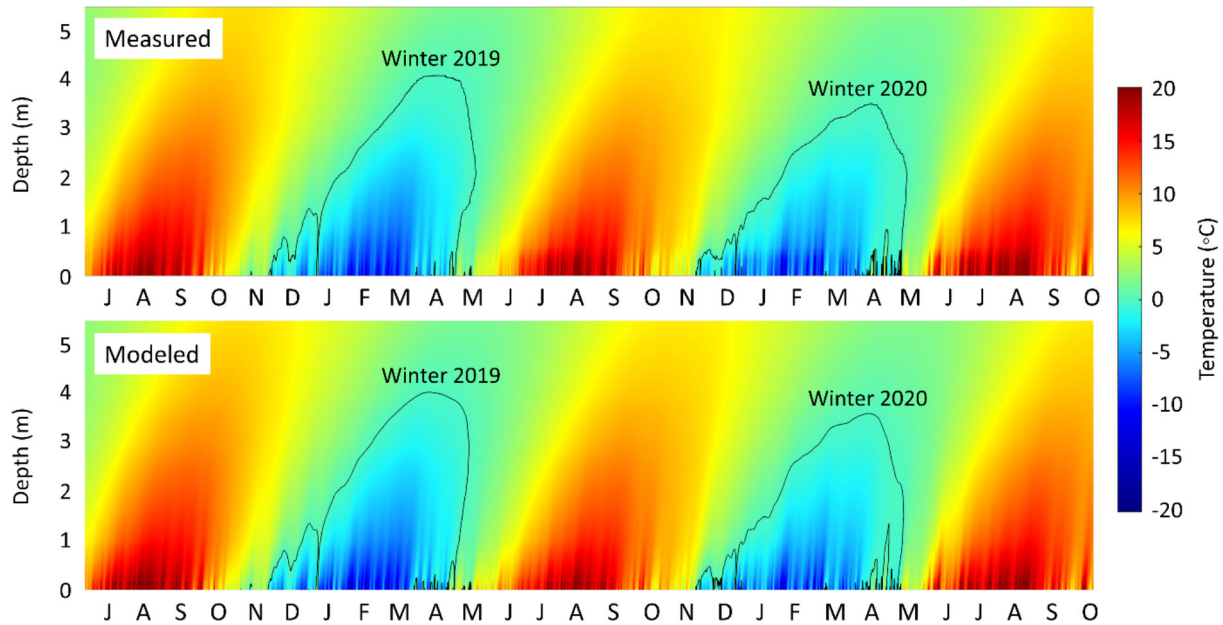


FIGURE 7 Measured and modelled thermal regime perpendicular to the surface of a flysch rockwall, 0–5.5 m in depth. Continuous black lines delineate the 0°C isotherm into the rockwall.

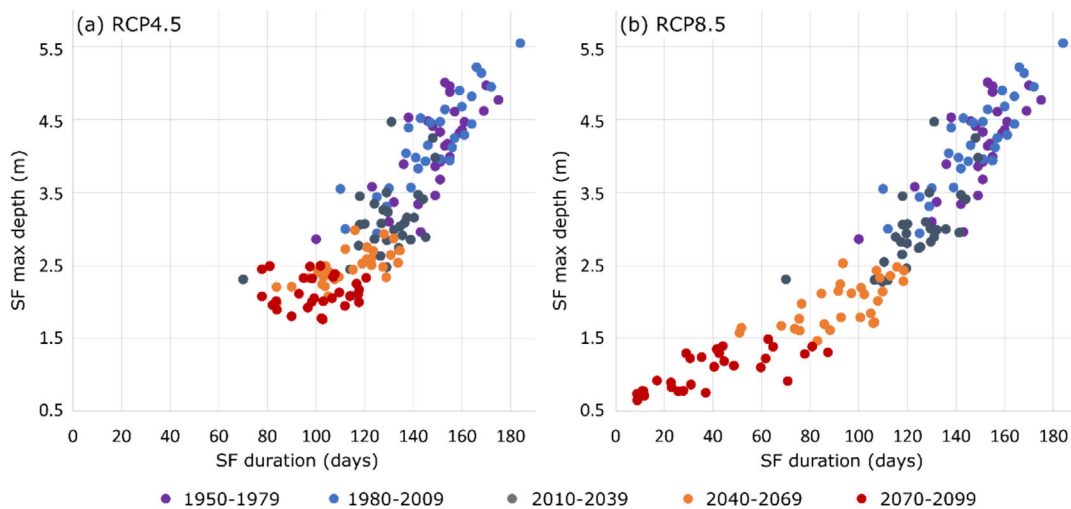


FIGURE 8 Duration and maximum depth of seasonal frost (SF), winters 1950–2100. From 1950 to 2020, the models used the air temperature measured at Cap-Madeleine. From 2021 onward, simulated temperatures from scenarios (a) RCP4.5 and (b) RCP8.5 were used.

damage at four preferential depths: at the surface and around 0.7, 1.3 and 2.7 m (Figure 11). The period 2010–2039 is expected to experience climate warming of over one degree Celsius compared with the two previous 30-year periods (Table 5). This warming would be enough to prevent ice lenses from forming deeper than 3.2 m (Figure 11). The following period (2040–2069) is expected to be marked by increased frost damage around 0.7 m in depth compared with historical periods and by decreased damage at greater depths (Figure 11). While this trend continues during the period 2070–2099 according to RCP4.5 (Figure 11a), effectiveness of frost cracking is predicted to decrease starting at 10 cm in depth considering RCP8.5 (Figure 11b). Climate warming could result in an increase in frost damage around 0.7 m in depth and a significant decrease past that depth. At the surface, frost cracking effectiveness is likely to remain as significant in the 2070–2099 period as in the historical periods (Figure 11).

5 | DISCUSSION

5.1 | Limitations and uncertainties

Uncertainties in modelling can come from not considered or misrepresented processes or errors in input data (Gubler et al., 2013; Gupta et al., 2005; Magnin et al., 2017), and it is inevitable that the model uncertainties increase at each step of our sequence: frost cracking is modelled from modelled rock temperature, which is itself modelled from modelled air temperature. The first limitation is that we only modelled air temperature for the future period and so we assumed that other parameters that have an influence on rock temperature as solar radiation or wind speed will not significantly be modified because of climate change. Nevertheless, as the modelled site is facing north and remains in constant shade from mid-October to mid-

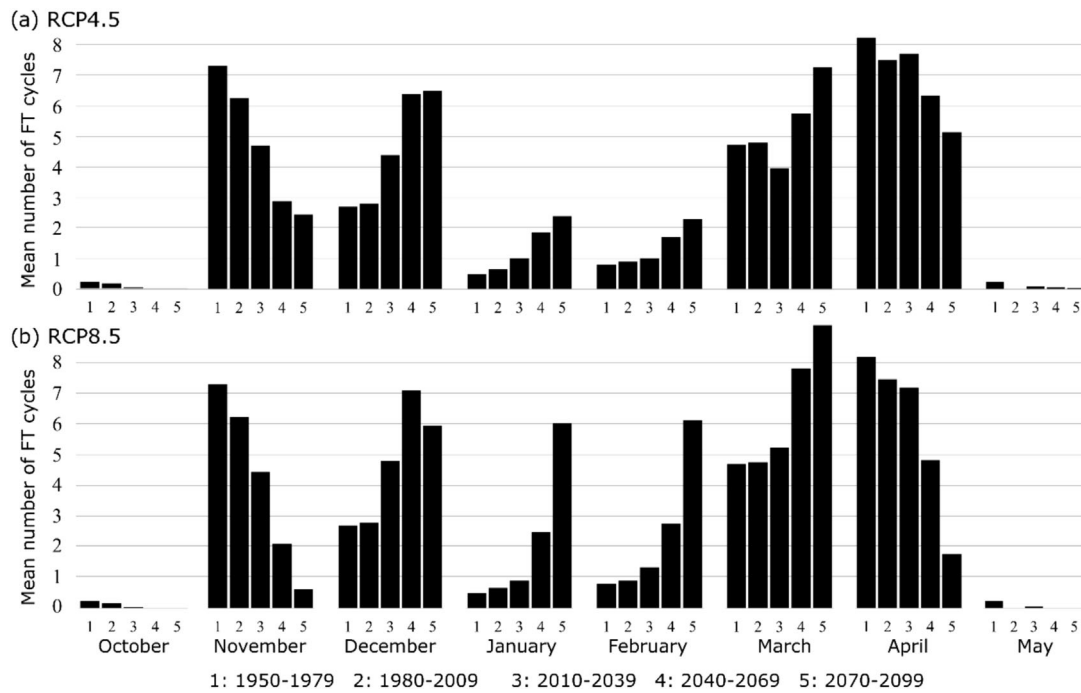


FIGURE 9 Mean monthly occurrence of sporadic freeze–thaw (FT) cycles during five 30-year periods from 1950 to 2099. The two first periods (1950–1979 and 1980–2009) were built with measured air temperature data, whereas the three last ones were partially (2010–2039) or fully (2040–2069, 2070–2099) built with simulated air temperature data from (a) RCP4.5 and (b) RCP8.5.

March and become only exposed to the late afternoon sun in spring, it is mostly affected by air temperature fluctuations in winter (Birien & Gauthier, 2023b). Snow cover can affect the rockwall surface temperature and thermal regime (Haberkorn et al., 2015, 2017; Phillips et al., 2016); however, the investigated rockwall is steep and not conducive to snow accumulation (Birien & Gauthier, 2023a) so we have neglected snow effect in our model.

Thermal conductivity, diffusivity and capacity drive the energy transfer inside the rock mass (Magnin et al., 2017), but other parameters that could affect this transfer have not been considered in our study. The presence of discontinuities that communicate with the surface and reach different depths into the rockwall can considerably increase heat flux through air convection (Gischig et al., 2011a, 2011b; Moore et al., 2011) or water advection (Gruber & Haeblerli, 2007; Hasler et al., 2011; Phillips et al., 2016). In the absence of air gaps along borehole instrumented with thermistor strings, these nonconductive heat transfers were not accounted for in our modelling approach. Nevertheless, it may concern other places in northern Gaspésie.

In porous and mostly saturated rock masses, the variable proportion (and state) of the interstitial ice or water can change the thermal properties over time (Magnin et al., 2017; Wegmann et al., 1998). The phase transition can also alter the speed of heat propagation through the rock by releasing or absorbing latent heat. These processes are included in WUFI[®] Pro (Karagiozis et al., 2001), but because we have used an invariable through time and depth degree of saturation of 80%, this process may be misrepresented. Water content into rock masses is very difficult to measure directly (Anderson et al., 2013), but some studies have shown that it remains quite high and relatively steady at depth (Graham et al., 2010; Langston et al., 2011; Sass, 2005). The water content value we have used is based on the work of Sass (2005), and the unknown availability of water remains an important assumption in our model.

The thermomechanical model developed by Rempel et al. (2016) assumes that frost damage is correlated with porosity increases under conditions where frost cracking takes place. One of the most important parameters in this model is the fracture toughness, which can be defined as the ability of rock to resist fracturing (Jian-An & Sijing, 1985) or in other words as the fracture energy consumption rate required to create new surfaces (Sun & Ouchterlony, 1986). The fracture toughness is closely linked with rock temperature and porosity (Atkinson, 1984; Dwivedi et al., 2000). We have used as input a constant value of fracture toughness for a fine-grained sandstone at 0°C from Dwivedi et al. (2000). The first limitation to use a constant value is that a decrease of 10°C from 0°C to –10°C results in an increase of the fracture toughness value of 11% (Dwivedi et al., 2000). Fortunately, temperature in the subsurface does not change as fast as at the rockwall surface (Figure 7). The second limitation is that we modelled the porosity change for 30-year periods, and the values obtained are cumulative. Draebing & Mayer (2021) have tested the sensitivity of this thermomechanical model, and by increasing the hydraulic permeability from 10^{–18} to 10^{–14} m², it shifts the porosity change by four orders of magnitude with values above 100% in only two winters. Our study, as well as the work of Draebing & Mayer (2021) or the work of Gauthier, Laliberté, et al. (2022b), Gauthier, Birien, & Meloche (2022a) show that the model developed by Rempel et al. (2016) is very sensitive to key parameter value adjustments as the fracture toughness, the hydraulic permeability or the initial crack length. Values of porosity change above 100% do not reflect the reality: when this value is reached, we assume that it attests to the development of crack at these depths. Then, the development of cracks and the detachment of blocks can lead to rockfalls. The new rockwall surface directly exposed to the atmosphere will be less porous and more resistant to fracturing. This erosion dynamics, which has not been taken into account in the modelling, is also in line

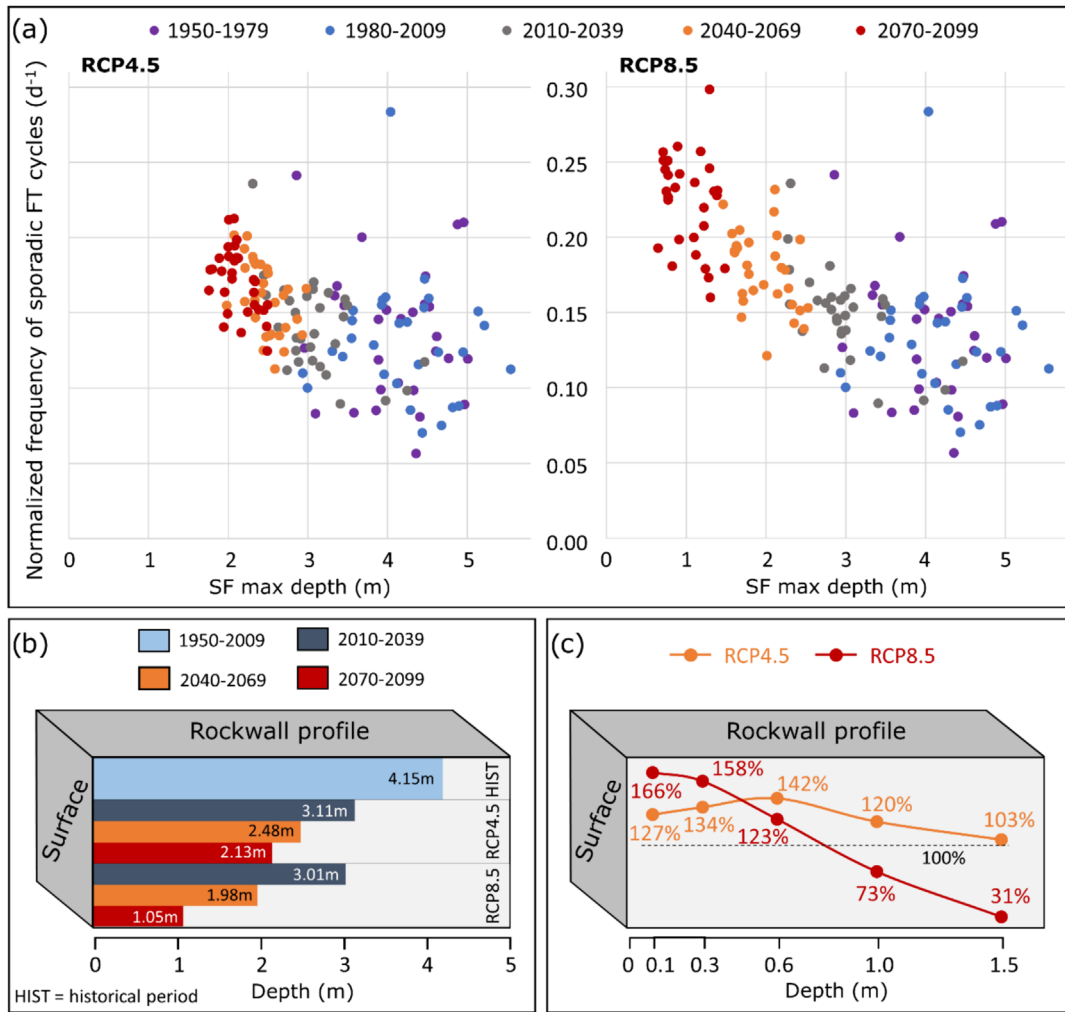


FIGURE 10 (a) Relationship between the normalized frequency of sporadic freeze–thaw (FT) cycles (or number of sporadic FT cycles per season divided by season length) (y-axis) and the maximum depth of seasonal frost (SF) (x-axis), from 1950 to 2099. (b) Mean maximum depth of SF during the historical period and for future periods according to RCP4.5 and RCP8.5, (c) relative FT cycles frequency (%) at different depths for the period 2070–2099 compared with the historical period (1950–2009) according to RCP4.5 and RCP8.5. Data from 1950 to 2020 were built with measured air temperature, whereas data from 2021 to 2099 were built with simulated air temperature based on RCP4.5 and RCP8.5.

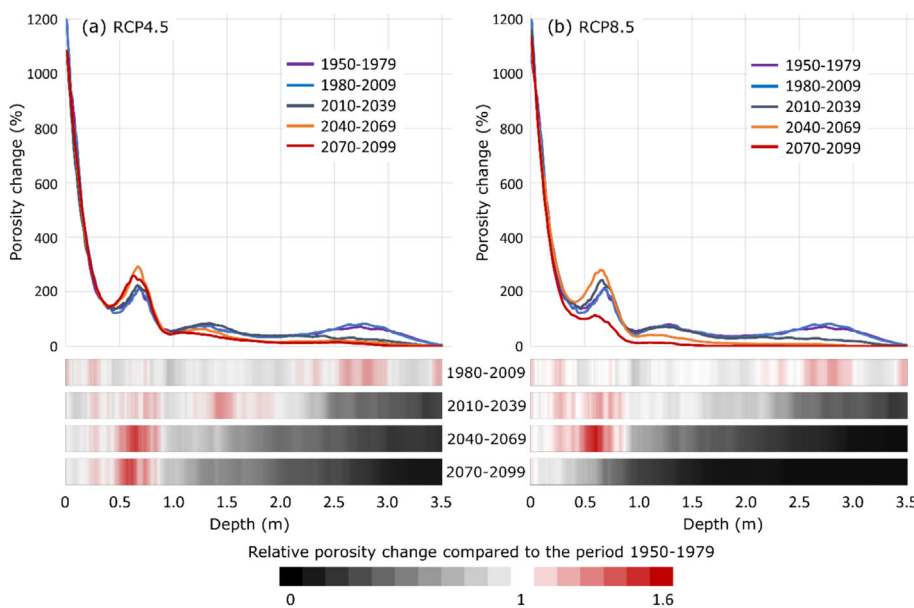


FIGURE 11 Simulations of cumulative porosity change (%) based on simulated rock temperatures for the five consecutive 30-year periods from 1950 to 2099 according to (a) RCP4.5 and (b) RCP8.5. The bars below the graphs represent the relative porosity change between the rockwall surface and the depth of 3.5 m for the periods 1980–2009, 2010–2039, 2040–2069 and 2070–2099 compared with the period 1950–1979.

with average rockwall retreat rates (2.8–5.5 mm year⁻¹) measured in flysch formations in northern Gaspésie (Birien & Gauthier, 2023a). Moreover, the frost cracking model proposed by Rempel et al. (2016) as well as those developed by Hales & Roering (2007) or by Anderson et al. (2013) or by Walder & Hallet (1985) assumes many thermal, hydrological and mechanical properties of rock (Draebing & Mayer, 2021). Because of these potential misrepresented properties, and as suggested by Draebing & Mayer (2021), the magnitude of frost cracking can only be interpreted in a qualitative way. Thus, we have limited our interpretation of the results to compare the effectiveness of frost cracking into the rockwall between the five 30-year studied periods rather than to interpret the order of magnitude of these values.

We have modelled air temperature locally and rock thermal regime or frost cracking on a micro-scale in the vicinity of the instrumented site. We consider that quantifying these processes on a micro-scale is an essential preliminary step to understand them on a macro-scale. Moreover, it is difficult to relate the physics of ice growth to rock breakdown by frost cracking at a regional scale because controlling hydraulic, thermal and mechanical parameters are difficult to obtain (Draebing & Mayer, 2021) and usually heterogeneous at this scale. Nevertheless, the instrumented (and modelled) site has been chosen to be as representative as possible of rockwalls at a region scale, especially because their great majority in northern Gaspésie overhang the St Lawrence estuary (same elevation and climate), are facing north, steep and composed of alternating strata of sandstone, greywacke, siltstone and shale of multi-decimetres thickness (Birien & Gauthier, 2023a, 2023b; Enos, 1969a, 1969b).

5.2 | Evolution of the frost processes ability to trigger rockfall in the global warming context

5.2.1 | From ice segregation to frost cracking

Based on our frost damage simulation results, ice lens formation could result in a preferential increase in porosity at the surface and at 0.7, 1.3 and 2.7 m in depth (Figure 11). These peaks of porosity change are indicators of frost-driven rock damage effectiveness and could be explained by the prolonged exposure at these depths to temperatures that promote water migration (Rempel et al., 2016). Global warming could have a major impact on these preferential depths of frost cracking by decreasing the maximum depth of SF by 1–2 m and shorten its duration by 1–3 months (Figure 8). Starting in the first decimetres below the surface, periods of rock temperatures within the range that promotes water migration and ice segregation could become scarce or even vanish. The frost cracking effectiveness should decrease as of 0.7 m in depth (RCP4.5) or as of 0.1 m in depth (RCP8.5) by the end of the 21st century (Figure 11).

Frost damage can also be induced by sporadic FT cycles through direct volumetric expansion of freezing water if the rock water saturation is above 91% (Deprez et al., 2020a, 2020b; Walder & Hallet, 1986). As explained by Matsuoka & Murton (2008), if the water completely fills spaces in rock and freezes *in situ*, then, theoretically, at a temperature of -22°C , ice growth can generate pressures up to 207 MPa inside cracks in a rock strong enough to withstand it. The maximum tensile strength of rock is one to two orders of

magnitude lower than 207 MPa, and even at warmer subzero temperatures, the maximum ice-induced stress is easily enough to fracture any rock (Matsuoka & Murton, 2008; Tsyrovich, 1975). However, Deprez et al. (2020a, 2020b) demonstrated that water crystallization in pores could drain water from adjacent micropores during short-term FT cycles. Thus, an initial critical saturation of only 70–80% is necessary to induce frost damage. As global warming appears to result in a higher FT cycle frequency near the surface and lower at greater depth in Northern Gaspésie (Figure 10c), the frost cracking effectiveness developed by volumetric expansion could intensify in shallower depth and be significantly reduced at greater depths.

5.2.2 | Effect on rockfall frequency and magnitude

It has been shown that FT cycles are strongly correlated with major deformations recorded by crackmetres in a siltstone segment of a rockwall in Northern Gaspésie (Birien & Gauthier, 2023b). While FT cycle occurrences only coincided with 4.7% of the 28-month time series, they corresponded to 40% of all identified major deformations (Birien & Gauthier, 2023b). In another work on the same rockwalls, it has been recorded that rockfall frequency was 11.7 times higher during FT cycles than during cold periods when the temperature remains below the freezing point (Birien & Gauthier, 2023a). The winter FT cycles were associated with a very high frequency of low-magnitude rockfalls, and the relation between winter FT cycles and higher-magnitude events was non-significant. This result is consistent with the fact that winter FT cycles influenced mainly the first 15 cm from the surface (Birien & Gauthier, 2023b). Other studies around the world have shown the relation between FT cycles depth and rockfalls (D'Amato et al., 2016b; Delonca et al., 2014b; Matsuoka, 2019). On the basis of the recent studies that have shown the relation between FT cycles and rock deformation (Birien & Gauthier, 2023b) as well as between FT cycles and rockfall (Birien & Gauthier, 2023a) in northern Gaspésie, we postulate that modern climate warming should increase the frequency of small rockfalls triggered by frost cracking (Figure 12).

The seasonal freezing phase is conducive to volumetric expansion and ice segregation processes that can induce frost cracking and so

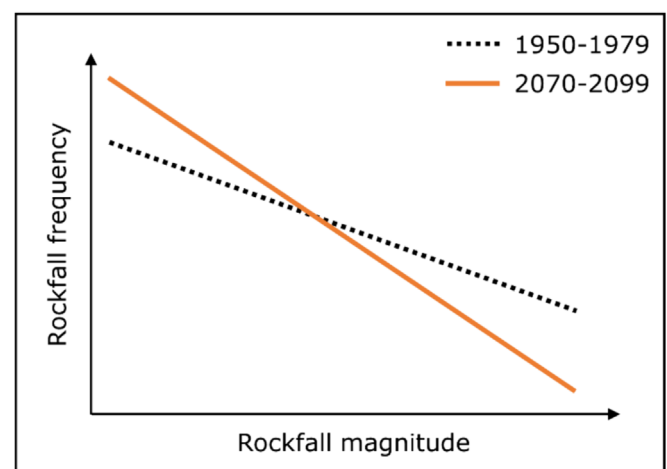


FIGURE 12 Conceptual relationship between frequency and magnitude of rockfall triggered by frost cracking in the context of global warming in environments subject to seasonal freezing.

fractures to open (Coutard & Francou, 1989; Matsuoka, 2008; Matsuoka & Sakai, 1999). However, cohesion at the ice-rock interface is generally sufficient to hold newly unstable blocks of rock in place; these blocks could fall later, when the ice melts in spring or summer (Fiorio et al., 2002; Krautblatter et al., 2013). The reduced cohesion associated with ice melt can be amplified by the increase in hydrostatic and in water-induced interstitial pressure. The water availability in spring could also be increased by water advection associated with snow cover melting and groundwater recharge (Gruber & Haeberli, 2007; Hasler et al., 2011; Phillips et al., 2016). Consequently, the mechanical action of this high-amplitude and long-term seasonal FT cycle (SF) has strong potential to destabilize rock portions (Dramis et al., 1995; Matsuoka, 2019; Matsuoka & Murton, 2008b; Wicczorek & Jäger, 1996). Indeed, the largest rockfalls in northern Gaspésie occur in spring when the SF thaws completely and during heavy rainfall events (Birien & Gauthier, 2023a). The relationship between rockfall magnitude and the depth of SF had also been reported by Matsuoka (2019) in a permafrost-free rockwall in the Japanese Alps. In Northern Gaspésie, only the SF reaches depths exceeding 1 m (Figure 7). Thus, global warming will likely result in a significant decrease in the maximum depth and duration of the SF (Figures 9 and 10). Because the frost cracking effectiveness should decrease starting at 70 cm in depth (RCP4.5) or even at 10 cm in depth (RCP8.5) by the end of the 21st century (Figure 11), frost cracking distribution into the rockwall should cease contributing to the development of large magnitude instabilities (Figure 12).

5.2.3 | Effect on monthly rockfall dynamic

The 21st century's climate changes are likely to result in the progressive disappearance of October and May frosts. Between 1950 and 2100, the frequency of sporadic FT cycles in November could be divided by 3 according to RCP4.5 and by 12 according to RCP8.5 (Figure 9). A decrease in both the effectiveness of frost cracking at the surface and the depth at which it operates can be expected. This

should reduce the frequency of rockfall triggered by frost cracking, particularly large magnitude rock instabilities (Figure 13a). In December, the frequency of sporadic FT cycles can be expected to double (Figure 9), but the freezing depth will decrease. By extension, the frequency of low magnitude rockfall triggered by FT cycles should increase while the frequency of higher magnitude instabilities should decrease (Figure 13b).

Historically, the winter period was particularly stable (Birien & Gauthier, 2023a; Laliberté et al., 2022) because the ice in cracks provided significant cohesion at the ice-rock interface to maintain unstable blocks in place (Fiorio et al., 2002). At the end of the 21st century, this period could be regularly interrupted by winter thaws. Compared with the period 1950–1979, their frequency could increase fivefold in January and threefold in February considering RCP4.5 and 12-fold and eightfold considering RCP8.5 (Figure 9). The volumetric expansion caused by short-term FT cycles can be expected to be exacerbated at the rockwall surface. This trend would extend to greater depths because the intensity and duration of winter thaws favour higher amplitude FT cycles. As a result, the rockfall frequency should increase proportionally with rockfall magnitude (Figure 13c,d). In March, the frequency of sporadic FT cycles would double (Figure 9), but the lower SF depth in winter (Figures 8 and 10b) would not favour FT cycles of very high amplitude. The frequency of rockfall could therefore substantially increase at the surface and significantly decrease at depth (Figure 13e). In April, sporadic FT cycles would be two times (RCP4.5) to five times (RCP8.5) less frequent (Figure 9), and the freezing depth of these cycles should decrease. This should result in a lower frequency of small magnitude rockfall and the end of frost cracking at greater depths (Figure 13f).

5.2.4 | Water availability and other processes

The role of water in the effectiveness of frost cracking has been discussed by many authors (Birien & Gauthier, 2023b; Bost, 2008; Davidson & Nye, 1985; Hall, 2004; Hallet et al., 1991;

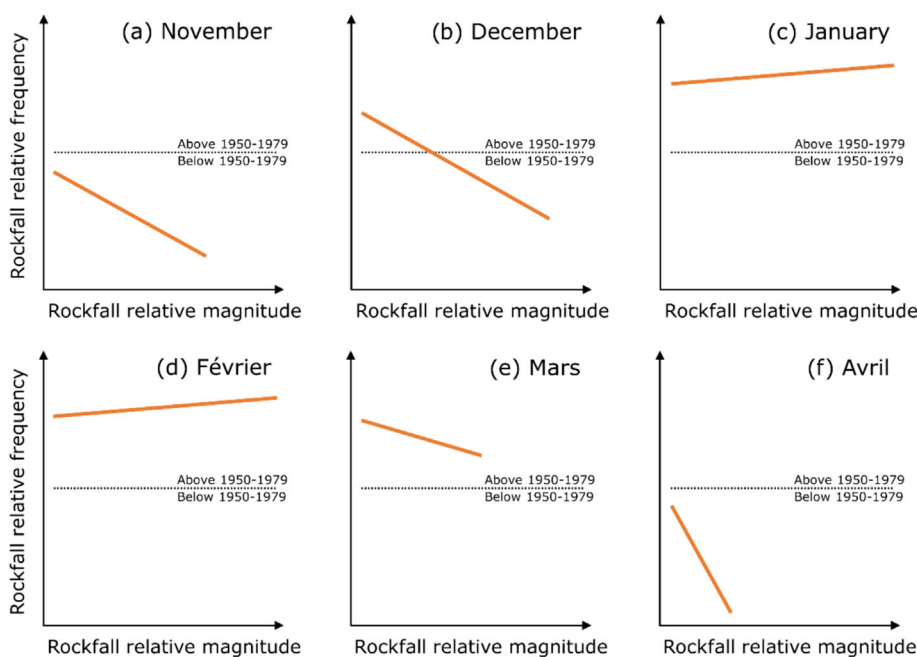


FIGURE 13 Conceptual representation of the relative frequency of varying magnitudes rockfalls triggered by frost cracking by the end of the century (2070–2099) compared with 1950–1979, in (a) November, (b) December, (c) January, (d) February, (e) March and (f) April in environments subject to seasonal frost.

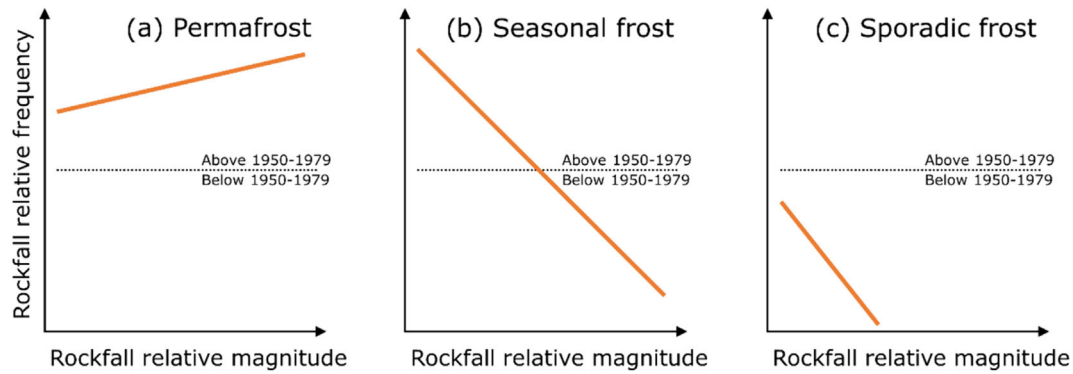


FIGURE 14 Conceptual representation of the relative frequency of varying magnitudes rockfalls triggered by frost cracking by the end of the century (2070–2099) compared with 1950–1979 in regions affected by (a) permafrost, (b) seasonal frost and (c) sporadic frost.

Matsuoka, 2001, 2008). Hall et al. (2002) note that the ability of FT cycles to alter rock is often overestimated, whereas the importance of available water is often underestimated. Birien & Gauthier (2023b) have shown that a high rock water content is a preliminary condition to the irreversibility of major deformation triggered by sporadic FT cycles. The increasing number of winter thaws in the late 21st century (Figure 9) should favour a greater availability of liquid water from melted interstitial ice and surface snow and from more frequent winter rain events (Gauthier, Laliberté, et al., 2022b; Hall et al., 2002; Rode et al., 2016). On the basis of these works, we assume that the water content should increase in winter with global warming.

The effectiveness of other processes than frost cracking could also be altered by modern climate change, especially because of the increased water availability. Rain events are particularly effective rockfall triggering factors (Birien & Gauthier, 2023a; D'Amato et al., 2016; Delonca et al., 2014; Matsuoka, 2019), and most other weathering processes are also dependent on liquid water inputs (Hall et al., 2002). This is particularly the case for dissolution, carbonation, hydrolysis and redox (Dixon & Thorn, 2005). Given the higher availability of liquid water in winter expected by the late 21st century, the effectiveness of these processes on rockwall surfaces and the resulting rates of weathering and erosion can be expected to rise. High amplitude thermal changes without freezing and water saturation can still cause subcritical cracking (Draebing, 2021; Eppes et al., 2016) and trigger rockfalls (Collins & Stock, 2016; Stock et al., 2012). Draebing (2021) has shown that climate change will affect the number and magnitude of these thermal changes, the associated stresses and so the rockfall dynamic.

5.3 | Frost-triggered rockfall dynamic on rockwalls affected by permafrost, by SF and by sporadic frost

In periglacial environments, permafrost has a significant influence on rockfall dynamics (Draebing et al., 2022; Paranunzio et al., 2016; Rabatel et al., 2008; Ravelle & Deline, 2011). Climate change leads to permafrost degradation, resulting at the very least in an increase in the thickness of its active layer in summer and even by the complete loss of relict permafrost (Farbrot et al., 2013; Gray et al., 2017; Gruber et al., 2004; Gruber & Haeberli, 2007; Hales & Roering, 2007). The increasing thickness of the active layer, along with a greater availability of liquid water (Rode et al., 2016), could result in increased rockfall

frequency and, above all, magnitude in periglacial environments (Draebing et al., 2022; Gobiet et al., 2014; Hartmeyer et al., 2020; Ravelle & Deline, 2011) (Figure 14a). However, following Murton et al. (2006), Murton, Kuras, et al. (2016a) and Murton, Ozouf, & Peterson (2016b) experiments, segregated ice tends to accumulate just below the permafrost table due to two-sided freezing. Thus, most intensive rockfall activity can be expected during the first stage of permafrost thawing, while further thawing of (possibly ice-poor) permafrost may reduce rockfall activity.

In rock masses subject to SF, global warming is likely to lead to more frequent sporadic FT cycles, particularly in winter (Figures 9 and 10), and greater liquid water availability (Rode et al., 2016). The periods of occurrence of these cycles should be shorter (Figure 9), and the freezing front should reach shallower depth (Figure 10). Compared with the historical period, late 21st century weather conditions would favour a rate of frost damage that is higher close to the rockwall surface but significantly lower at depth (Figure 11). An increased frequency of small magnitude rockfall triggered by frost cracking and a decreased frequency of higher magnitude instabilities can be expected (Figure 14b).

Some midlatitude climates such as those of the low elevation mountain in the European Alps (D'Amato et al., 2016; Rode et al., 2016), the Japanese Alps (Matsuoka, 1991), the Sierra Nevada (Wieczorek & Jäger, 1996) or the Canadian coast mountain (van Veen et al., 2017) are more temperate than those of northern Gaspésie (Beck et al., 2018). They experience a higher frequency of sporadic FT cycles, shorter winter periods and an absence of SF. In this context, frequent winter temperature oscillations around the freezing point promote the development of small magnitude rock instabilities (D'Amato et al., 2016; Delonca et al., 2014; Kromer et al., 2018; Macciotta et al., 2015; van Veen et al., 2017). Climate warming by the end of the 21st century in these regions can be expected to reduce the frequency and amplitude of winter FT cycles or even eliminate them (Rode et al., 2016). This should reduce the frequency of small magnitude rockfall triggered by frost cracking (Figure 14c).

6 | CONCLUSION

Depending on the scenario, the climate of the northern Gaspé Peninsula can be expected to warm by 3.3°C (RCP4.5) to 6.2°C (RCP8.5) during the 21st century. This rapid warming will likely result in a significant decrease in the maximum depth of SF, a truncated period of occurrence

of sporadic FT cycles and a very substantial increase in their frequency in winter. Compared with the historical period (1950–2009) and following RCP4.5, frost cracking effectiveness should intensify around 70 cm in depth and disappear beyond that. According to RCP8.5, frost cracking effectiveness is predicted to decrease as of 10 cm in depth. In rock masses subject to seasonal freezing, the changes predicted in frost cracking process effectiveness by the end of the 21st century should favour the development of small magnitude rock instabilities over high magnitude ones. The frequency of rockfall triggered by sporadic FT cycles could grow considerably in winter but be significantly diminished in fall and spring. In the initial phase of permafrost thawing, the increasing thickness of the active layer, along with a likely greater availability of liquid water, should result in increased rockfall frequency and, above all, magnitude. In warmer environments, where rockslope are only affected by sporadic FT cycle, global warming is likely to diminish the frequency and intensity of winter FT cycles. This should also reduce the frequency of small magnitude rockfalls triggered by those cycles. Other mechanical and chemical weathering processes effectiveness could be altered by climate warming and change the rockwall retreat rate and thus the frequency and magnitude of rock instabilities in the late 21st century. No conclusion from our work can be given on this overall rockfall dynamic in a climate change context because we only focused on the frost processes influence. Further studies are required to establish links between climatic drivers, weathering processes and rockfalls.

AUTHOR CONTRIBUTIONS

Tom Birien made the field work, developed the data processing, carried out the data analysis and wrote the manuscript. Francis Gauthier made the funding acquisition and helped to develop the initial idea and to prepare the manuscript. Francis Meloche did the thermomechanical simulations presented in Figure 11. All authors contributed to the review process.

ACKNOWLEDGEMENTS

We acknowledge the World Climate Research Programme's Working Group on Regional Climate and the Working Group on Coupled Modelling, former coordinating body of CORDEX and responsible panel for CMIP5. We also thank the climate modelling groups (listed in Table 1 of this paper) for producing and making available their model output. We also acknowledge the U.S. Department of Defense ESTCP for its support of the NA-CORDEX data archive. We are grateful for the work and support of Guillaume Dueymes for the preparation of the data and their distribution and of the Centre pour l'Étude et la Simulation du Climat à l'Échelle Régionale (ESCER) at the Université du Québec à Montréal (UQAM). Finally, we thank the Laboratoire ouvert de géothermie (LOG) of the Institut National de la Recherche Scientifique (INRS) for their help, and we are particularly grateful for the assistance provided by Nicolo Giordano. This work was financially supported by the Ministère des Transports du Québec (MTQ) and by the Natural Sciences and Engineering Research Council of Canada (NSERC).

DATA AVAILABILITY STATEMENT

All the data collected during this study are available on request. Codes were only used to realize the Figures 7 and 11 and can also be sent on request.

ORCID

Tom Birien  <https://orcid.org/0000-0002-2572-350X>

REFERENCES

- Albert, K., Schulze, M., Franz, C., Koenigsdorff, R. & Zosseder, K. (2017) Thermal conductivity estimation model considering the effect of water saturation explaining the heterogeneity of rock thermal conductivity. *Geothermics*, 66, 1–12. Available from: <https://doi.org/10.1016/j.geothermics.2016.11.006>
- Alvioli, M., Melillo, M., Guzzetti, F., Rossi, M., Palazzi, E., von Hardenberg, J., et al. (2018) Implications of climate change on landslide hazard in Central Italy. *Science of the Total Environment*, 630, 1528–1543. Available from: <https://doi.org/10.1016/j.scitotenv.2018.02.315>
- Andersland, O.B. & Ladanyi, B. (2003) *Frozen ground engineering*. Hoboken, NJ: John Wiley & Sons.
- Anderson, R.S. (1998) Near-surface thermal profiles in alpine bedrock: implications for the frost weathering of rock. *Arctic and Alpine Research*, 30(4), 362–372. Available from: <https://doi.org/10.2307/1552008>
- Anderson, R.S., Anderson, S.P. & Tucker, G.E. (2013) Rock damage and regolith transport by frost: An example of climate modulation of the geomorphology of the critical zone. *Earth Surface Processes and Landforms*, 38(3), 299–316. Available from: <https://doi.org/10.1002/esp.3330>
- Atkinson, B.K. (1984) Subcritical crack growth in geological materials. *Journal of Geophysical Research*, 89(B6), 4077–4114. Available from: <https://doi.org/10.1029/jb089ib06p04077>
- Atkinson, B.K. & Rawlings, R.D. (1981) Acoustic emission during stress corrosion cracking in rocks. *Earthquake Prediction: An International Review. Maurice Ewing Series 4*, American Geophysical Union, pp. 605–616.
- Beck, H.E., Zimmermann, N.E., McVicar, T.R., Vergopolan, N., Berg, A. & Wood, E.F. (2018) Present and future Köppen-Geiger climate classification maps at 1-km resolution. *Scientific Data*, 5, 1–12. Available from: <https://doi.org/10.1038/sdata.2018.214>
- Birien, T. & Gauthier, F. (2023a) Assessing the relationship between weather conditions and rockfall using terrestrial laser scanning to improve risk management. *Natural Hazards and Earth System Sciences*, 23(1), 343–360. Available from: <https://doi.org/10.5194/nhess-23-343-2023>
- Birien, T. & Gauthier, F. (2023b) Influence of climate-dependent variables on deformation and differential erosion of stratified sedimentary rocks. *Geomorphology*, 421, 108518. Available from: <https://doi.org/10.1016/j.geomorph.2022.108518>
- Bost, M. (2008). *Altération par le gel des massifs rocheux : Etude expérimentale et modélisation des mécanismes de génération des contraintes dans les fissures* (Issue November) [Ecole des Ponts ParisTech]. Champs-sur-Marne (France): Ecole des Ponts ParisTech. <https://pastel.archives-ouvertes.fr/tel-00360420>
- Budetta, P. (2004) Assessment of rockfall risk along roads. *Natural Hazards and Earth System Sciences*, 4(1), 71–81. Available from: <https://doi.org/10.5194/nhess-4-71-2004>
- Christensen, O.B., Drews, M., Christensen, J.H., Dethloff, K., Ketelsen, K., Hebestadt, I., et al. (2007) The HIRHAM Regional Climate Model Version 5 (beta). In: *Technical report 06-17*, Vol. 5. Copenhagen, Denmark: Danish Meteorological Institute.
- Collins, M., Knutti, R., Arblaster, J., Dufresne, J.-L., Fichefet, T., Friedlingstein, P., et al. (2013) Long-term climate change: projections, commitments and irreversibility. In: *Climate change 2013 the physical science basis: working group I contribution to the fifth assessment report of the intergovernmental panel on climate change*. Cambridge, Royaume-Uni: Cambridge University Press. <https://doi.org/10.1017/CBO9781107415324.024>
- Collins, B.D. & Stock, G.M. (2016) Rockfall triggering by cyclic thermal stressing of exfoliation fractures. *Nature Geoscience*, 9(5), 395–400. Available from: <https://doi.org/10.1038/ngeo2686>
- Coutard, J.P. & Francou, B. (1989) Rock temperature measurements in two alpine environments: implications for frost shattering. *Arctic and*

- Alpine Research, 21(4), 399–416. Available from: <https://doi.org/10.2307/1551649>
- Crosta, G.B. & Clague, J.J. (2009) Dating, triggering, modelling, and hazard assessment of large landslides. *Geomorphology*, 103(1), 14. Available from: <https://doi.org/10.1016/j.geomorph.2008.04.007>
- Crozier, M.J. (2010) Deciphering the effect of climate change on landslide activity: a review. *Geomorphology*, 124(3–4), 260–267. Available from: <https://doi.org/10.1016/j.geomorph.2010.04.009>
- D'Amato, J., Hantz, D., Guerin, A., Jaboyedoff, M., Baillet, L. & Mariscal, A. (2016) Influence of meteorological factors on rockfall occurrence in a middle mountain limestone cliff. *Natural Hazards and Earth System Sciences*, 16(3), 719–735. Available from: <https://doi.org/10.5194/nhess-16-719-2016>
- Davidson, G.P. & Nye, J.F. (1985) A photoelastic study of ice pressure in rock cracks. *Cold Regions Science and Technology*, 11(2), 141–153. Available from: [https://doi.org/10.1016/0165-232X\(85\)90013-8](https://doi.org/10.1016/0165-232X(85)90013-8)
- Delonca, A., Gunzburger, Y. & Verdel, T. (2014) Statistical correlation between meteorological and rockfall databases. *Natural Hazards and Earth System Sciences*, 14(8), 1953–1964. Available from: <https://doi.org/10.5194/nhess-14-1953-2014>
- Deprez, M., De Kock, T., De Schutter, G. & Cnudde, V. (2020a) A review on freeze-thaw action and weathering of rocks. *Earth-Science Reviews*, 203(February), 103143. Available from: <https://doi.org/10.1016/j.earscirev.2020.103143>
- Deprez, M., De Kock, T., De Schutter, G. & Cnudde, V. (2020b) The role of ink-bottle pores in freeze-thaw damage of oolitic limestone. *Construction and Building Materials*, 246, 118515. Available from: <https://doi.org/10.1016/j.conbuildmat.2020.118515>
- Dixon, J.C. & Thorn, C.E. (2005) Chemical weathering and landscape development in mid-latitude alpine environments. *Geomorphology*, 67(1–2 SPEC. ISS), 127–145. Available from: <https://doi.org/10.1016/j.geomorph.2004.07.009>
- Draebing, D. (2021) Identification of rock and fracture kinematics in high alpine rockwalls under the influence of elevation. *Earth Surface Dynamics*, 9(4), 977–994. Available from: <https://doi.org/10.5194/esurf-9-977-2021>
- Draebing, D. & Krautblatter, M. (2019) The efficacy of frost weathering processes in Alpine Rockwalls. *Geophysical Research Letters*, 46(12), 6516–6524. Available from: <https://doi.org/10.1029/2019GL081981>
- Draebing, D. & Mayer, T. (2021) Topographic and geologic controls on frost cracking in Alpine Rockwalls. *Journal of Geophysical Research - Earth Surface*, 126(6), e2021JF006163. Available from: <https://doi.org/10.1029/2021JF006163>
- Draebing, D., Mayer, T., Jacobs, B. & McColl, S.T. (2022) Alpine rockwall erosion patterns follow elevation-dependent climate trajectories. *Communications Earth & Environment*, 3(1), 1–12. Available from: <https://doi.org/10.1038/s43247-022-00348-2>
- Dramis, F., Govi, M., Guglielmin, M. & Mortara, G. (1995) Mountain permafrost and slope instability in the Italian Alps: the Val Pola landslide. *Permafrost and Periglacial Processes*, 6(1), 73–81. Available from: <https://doi.org/10.1002/ppp.3430060108>
- Dwivedi, R.D., Soni, A.K., Goel, R.K. & Dube, A.K. (2000) Fracture toughness of rocks under sub-zero temperature conditions. *International Journal of Rock Mechanics and Mining Sciences*, 37(8), 1267–1275. Available from: [https://doi.org/10.1016/S1365-1609\(00\)00051-4](https://doi.org/10.1016/S1365-1609(00)00051-4)
- Enos, P. (1969a) Anatomy of a flysch. *Journal of Sedimentary Petrology*, 39(2), 680–723.
- Enos, P. (1969b) In: Geological Society of America INC. (Ed.) *Cloridorme formation, middle ordovician flysch, Northern Gaspé peninsula, Québec*. Boulder, USA: Geological Society of America.
- Environment Canada. (2021). *Compilation des données historiques à la station météorologique de Cap-Madeleine*. Ottawa, Canada: Gouvernement du Canada. https://climat.meteo.gc.ca/historical_data/search_historic_data_f.html
- Eppes, M.C., Magi, B., Hallet, B., Delmelle, E., Mackenzie-Helnwein, P., Warren, K., et al. (2016) Deciphering the role of solar-induced thermal stresses in rock weathering. *Bulletin of the Geological Society of America*, 128(9–10), 1315–1338. Available from: <https://doi.org/10.1130/B31422.1>
- Fahey, B.D. & Lefebure, T.H. (1988) The freeze-thaw weathering regime at a section of the Niagara escarpment on the Bruce Peninsula, Southern Ontario, Canada. *Earth Surface Processes and Landforms*, 13(4), 293–304. Available from: <https://doi.org/10.1002/esp.3290130403>
- Farbrot, H., Isaksen, K., Etmüller, B. & Gislén, K. (2013) Ground thermal regime and permafrost distribution under a changing climate in Northern Norway. *Permafrost and Periglacial Processes*, 24(1), 20–38. Available from: <https://doi.org/10.1002/ppp.1763>
- Fiorio, B., Meyssonier, J. & Boulon, M. (2002) Experimental study of the friction of ice over concrete under simplified ice-structure interaction conditions. *Canadian Journal of Civil Engineering*, 29(3), 347–359. Available from: <https://doi.org/10.1139/102-012>
- Gariano, S.L. & Guzzetti, F. (2016) Landslides in a changing climate. *Earth-Science Reviews*, 162, 227–252. Available from: <https://doi.org/10.1016/j.earscirev.2016.08.011>
- Gauthier, F., Allard, M. & Héту, B. (2015) Ice wall growth and decay: meteorological analysis and modelling. *Permafrost and Periglacial Processes*, 26(1), 84–102. Available from: <https://doi.org/10.1002/ppp.1835>
- Gauthier, F., Birien, T. & Meloche, F. (2022a) Dynamique des parois de flysch (partie1): développement des instabilités et modes de rupture. In: *8e Conférence Canadienne Sur La Géotechnique et Les Risques Naturels - Géorisques*, Vol. 8. Canada: Société canadienne de géotechnique, pp. 373–381.
- Gauthier, F., Laliberté, J., Birien, T., Boulet, Y., Meloche, F., & Buffin-Bélanger, T. (2022b). Influence des variables météorologiques et des changements climatiques sur l'occurrence, la fréquence et la magnitude des mouvements de versant (avalanche de neige, chute de blocs de glace et chute de pierre) affectant certains tronçons des routes 132 et 198 dans le nord de la Gaspésie R798.1. <http://www.bv.transports.gouv.qc.ca/mono/1301736.pdf>
- Gauthier, F., Montagnat, M., Weiss, J., Allard, M. & Héту, B. (2013) Ice cascade growth and decay: a thermodynamic approach. *Journal of Glaciology*, 59(215), 507–523. Available from: <https://doi.org/10.3189/2013JoG12J206>
- Gischig, V.S., Moore, J.R., Evans, K.F., Amann, F. & Loew, S. (2011a) Thermomechanical forcing of deep rock slope deformation: 1. Conceptual study of a simplified slope. *Journal of Geophysical Research - Earth Surface*, 116(4), 1–18. Available from: <https://doi.org/10.1029/2011JF002006>
- Gischig, V.S., Moore, J.R., Evans, K.F., Amann, F. & Loew, S. (2011b) Thermomechanical forcing of deep rock slope deformation: 2. The Randa rock slope instability. *Journal of Geophysical Research - Earth Surface*, 116(4), 1–17. Available from: <https://doi.org/10.1029/2011JF002007>
- Gobiet, A., Kotlarski, S., Beniston, M., Heinrich, G., Rajczak, J. & Stoffel, M. (2014) 21st century climate change in the European Alps—a review. *Science of the Total Environment*, 493, 1138–1151. Available from: <https://doi.org/10.1016/j.scitotenv.2013.07.050>
- Graham, R.C., Rossi, A.M. & Hubbert, K.R. (2010) Rock to regolith conversion: producing hospitable substrates for terrestrial ecosystems. *GSA Today*, 20(2), 4–9. Available from: <https://doi.org/10.1130/GSAT57A.1>
- Gray, J., Davesne, G., Fortier, D. & Godin, E. (2017) The thermal regime of mountain permafrost at the summit of Mont Jacques-Cartier in the Gaspé peninsula, Québec, Canada: a 37 year record of fluctuations showing an overall warming trend. *Permafrost and Periglacial Processes*, 28(1), 266–274. Available from: <https://doi.org/10.1002/ppp.1903>
- Gruber, S. & Haeblerli, W. (2007) Permafrost in steep bedrock slopes and its temperatures-related destabilization following climate change. *Journal of Geophysical Research - Earth Surface*, 112(2), F02S18. Available from: <https://doi.org/10.1029/2006JF000547>
- Gruber, S., Hoelzle, M. & Haeblerli, W. (2004) Permafrost thaw and destabilization of Alpine rock walls in the hot summer of 2003. *Geophysical Research Letters*, 31(13), 1–4. Available from: <https://doi.org/10.1029/2004GL020051>
- Gubler, S., Endrizzi, S., Gruber, S. & Purves, R.S. (2013) Sensitivities and uncertainties of modeled ground temperatures in mountain environments. *Geoscientific Model Development*, 6(4), 1319–1336. Available from: <https://doi.org/10.5194/gmd-6-1319-2013>

- Gunzburger, Y., Merrien-Soukatchoff, V. & Guglielmi, Y. (2005) Influence of daily surface temperature fluctuations on rock slope stability: case study of the Rochers de Valabres slope (France). *International Journal of Rock Mechanics and Mining Sciences*, 42(3), 331–349. Available from: <https://doi.org/10.1016/j.ijrmm.2004.11.003>
- Gupta, H.V., Beven, K. & Wagener, T. (2005) *Model calibration and uncertainty estimation*. Hoboken, NJ: John Wiley & Sons.
- Haberkorn, A., Hoelzle, M., Phillips, M. & Kenner, R. (2015) Snow as a driving factor of rock surface temperatures in steep rough rock walls. *Cold Regions Science and Technology*, 118, 64–75. Available from: <https://doi.org/10.1016/j.coldregions.2015.06.013>
- Haberkorn, A., Wever, N., Hoelzle, M., Phillips, M., Kenner, R., Bavay, M., et al. (2017) Distributed snow and rock temperature modelling in steep rock walls using Alpine3D. *The Cryosphere*, 11(1), 585–607. Available from: <https://doi.org/10.5194/tc-11-585-2017>
- Hales, T.C. & Roering, J.J. (2007) Climatic controls on frost cracking and implications for the evolution of bedrock landscapes. *Journal of Geophysical Research - Earth Surface*, 112(2), 1–14. Available from: <https://doi.org/10.1029/2006JF000616>
- Hall, K. (2004) Evidence for freeze-thaw events and their implications for rock weathering in northern Canada. *Earth Surface Processes and Landforms*, 29(1), 43–57. Available from: <https://doi.org/10.1002/esp.1012>
- Hall, K., Thorn, C.E., Matsuoka, N. & Prick, A. (2002) Weathering in cold regions: some thoughts and perspectives. *Progress in Physical Geography*, 26(4), 577–603. Available from: <https://doi.org/10.1191/0309133302pp353ra>
- Hallet, B., Walder, J.S. & Stubbs, C.W. (1991) Weathering by segregation ice growth in microcracks at sustained subzero temperatures: verification from an experimental study using acoustic emissions. *Permafrost and Periglacial Processes*, 2(4), 283–300. Available from: <https://doi.org/10.1002/ppp.3430020404>
- Haque, U., da Silva, P.F., Devoli, G., Pilz, J., Zhao, B., Khaloua, A., et al. (2019) The human cost of global warming: deadly landslides and their triggers (1995–2014). *Science of the Total Environment*, 682, 673–684. Available from: <https://doi.org/10.1016/j.scitotenv.2019.03.415>
- Harris, C., Arenson, L.U., Christiansen, H.H., Eitzelmlüller, B., Frauenfelder, R., Gruber, S., et al. (2009) Permafrost and climate in Europe: monitoring and modelling thermal, geomorphological and geotechnical responses. *Earth-Science Reviews*, 92(3–4), 117–171. Available from: <https://doi.org/10.1016/j.earscirev.2008.12.002>
- Hartmann, D.L., Klein Tank, A.M.G., Rusticucci, M., Alexander, L.V., Brönnimann, S., Charabi, Y., et al. (2013) IPCC Climate Change 2013: The Physical Science Basis. Chapter 2: Observations: atmosphere and Surface. In: *Climate change 2013 the physical science basis: working group I contribution to the fifth assessment report of the intergovernmental panel on climate change*, Vol. 9781107057. Cambridge, UK and New York, USA: Cambridge University, pp. 159–254.
- Hartmeyer, I., Keuschnig, M., Delleske, R., Krautblatter, M., Lang, A., Schrott, L., et al. (2020) A 6-year lidar survey reveals enhanced rockwall retreat and modified rockfall magnitudes/frequencies in deglaciating cirques. *Earth Surface Dynamics*, 8, 753–768. Available from: <https://doi.org/10.5194/esurf-8-753-2020>
- Hasler, A., Gruber, S., Font, M. & Dubois, A. (2011) Advective heat transport in frozen rock clefts: conceptual model, laboratory experiments and numerical simulation. *Permafrost and Periglacial Processes*, 22(4), 378–389. Available from: <https://doi.org/10.1002/ppp.737>
- Héту, B. & Gray, J.T. (1985) Le modèle d'érosion glaciaire de la Gaspésie septentrionale. *Géographie Physique et Quaternaire*, 39(1), 47–66. Available from: <https://doi.org/10.7202/032584ar>
- Héту, B. & Vandelac, P. (1989) La dynamique des éboulis schisteux au cours de l'hiver, Gaspésie septentrionale, Québec. *Géographie Physique et Quaternaire*, 43(3), 389–406. Available from: <https://doi.org/10.7202/032791ar>
- Huggel, C. (2009) Recent extreme slope failures in glacial environments: effects of thermal perturbation. *Quaternary Science Reviews*, 28(11–12), 1119–1130. Available from: <https://doi.org/10.1016/j.quascirev.2008.06.007>
- Huggel, C., Clague, J.J. & Korup, O. (2012) Is climate change responsible for changing landslide activity in high mountains? *Earth Surface Processes and Landforms*, 37(1), 77–91. Available from: <https://doi.org/10.1002/esp.2223>
- Hungr, O., Evans, S.G. & Hazzard, J. (1999) Magnitude and frequency of rock falls and rock slides along the main transportation corridors of southwestern British Columbia. *Canadian Geotechnical Journal*, 36(2), 224–238. Available from: <https://doi.org/10.1139/t98-106>
- ISRM. (1979) Suggested methods for determining water content, porosity, density absorption and related properties and swelling and slake-durability index properties. *International Journal of Rock Mechanics and Mining Science and Geomechanics Abstracts*, 16, 141–156.
- Jian-An, H. & Sijing, W. (1985) An experimental investigation concerning the comprehensive fracture toughness of some brittle rocks. *International Journal of Rock Mechanics and Mining Science and Geomechanics Abstracts*, 22(2), 99–104. Available from: [https://doi.org/10.1016/0148-9062\(85\)92331-9](https://doi.org/10.1016/0148-9062(85)92331-9)
- Karagiozis, A., Künzel, H. & Holm, A. (2001) WUFI-ORNL/IBP—a North American Hygrothermal model. The performance of Exterior Envelopes of Whole Buildings VIII International Conference. Clearwater Beach, FL.
- Korup, O., Görüm, T. & Hayakawa, Y. (2012) Without power? Landslide inventories in the face of climate change. *Earth Surface Processes and Landforms*, 37(1), 92–99. Available from: <https://doi.org/10.1002/esp.2248>
- Krautblatter, M., Funk, D. & Günzel, F.K. (2013) Why permafrost rocks become unstable: a rock-ice-mechanical model in time and space. *Earth Surface Processes and Landforms*, 38(8), 876–887. Available from: <https://doi.org/10.1002/esp.3374>
- Kromer, R.A., Rowe, E., Hutchinson, J., Lato, M. & Abellán, A. (2018) Rockfall risk management using a pre-failure deformation database. *Landslides*, 15(5), 847–858. Available from: <https://doi.org/10.1007/s10346-017-0921-9>
- Lachenbruch, A.H., Cladouhos, T.T. & Saltus, R.W. (1988) Permafrost temperature and the changing climate. In: *Fifth international conference on permafrost*, Vol. 3. Trondheim, Norway: Tapir Academic Press, pp. 9–17.
- Labiberté, J., Gauthier, F. & Birien, T. (2022) Dynamique des parois de flysch (partie3): prévision des chutes de pierres. In: Société canadienne de géotechnique. (Ed.) *8e conférence canadienne sur la géotechnique et les risques naturels - Géorisques*, Vol. 8. Canada: Société canadienne de géotechnique.
- Langston, A.L., Tucker, G.E., Anderson, R.S. & Anderson, S.P. (2011) Exploring links between vadose zone hydrology and chemical weathering in the Boulder Creek critical zone observatory. *Applied Geochemistry*, 26(SUPPL), S70–S71. Available from: <https://doi.org/10.1016/j.apgeochem.2011.03.033>
- Lippmann and Rauen GbR. (2022). *Thermal conductivity scanning*. Schauffling, Germany: Lippmann Geophysikalische Messgeräte. <http://www.geophysik-dr-rauen.de/tcscan/index.html>
- Macciotta, R., Martin, C.D., Edwards, T., Cruden, D.M. & Keegan, T. (2015) Quantifying weather conditions for rock fall hazard management. *Georisk*, 9(3), 171–186. Available from: <https://doi.org/10.1080/17499518.2015.1061673>
- Magnin, F., Josnin, J.Y., Raveland, L., Pergaud, J., Pohl, B. & Deline, P. (2017) Modelling rock wall permafrost degradation in the Mont Blanc massif from the LIA to the end of the 21st century. *The Cryosphere*, 11(4), 1813–1834. Available from: <https://doi.org/10.5194/tc-11-1813-2017>
- Martynov, A., Laprise, R., Sushama, L., Winger, K., Šeparović, L. & Dugas, B. (2013) Reanalysis-driven climate simulation over CORDEX North America domain using the Canadian Regional Climate Model, version 5: model performance evaluation. *Climate Dynamics*, 41(11–12), 2973–3005. Available from: <https://doi.org/10.1007/s00382-013-1778-9>
- Matsuoka, N. (1991) A model of the rate of frost shattering: application to field data from Japan, Svalbard and Antarctica. *Permafrost and Periglacial Processes*, 2(4), 271–281. Available from: <https://doi.org/10.1002/ppp.3430020403>
- Matsuoka, N. (2001) Direct observation of frost wedging in alpine bedrock. *Earth Surface Processes and Landforms*, 26(6), 601–614. Available from: <https://doi.org/10.1002/esp.208>
- Matsuoka, N. (2008) Frost weathering and rockwall erosion in the south-eastern Swiss Alps: long-term (1994–2006) observations.

- Geomorphology*, 99(1–4), 353–368. Available from: <https://doi.org/10.1016/j.geomorph.2007.11.013>
- Matsuoka, N. (2019) A multi-method monitoring of timing, magnitude and origin of rockfall activity in the Japanese Alps. *Geomorphology*, 336, 65–76. Available from: <https://doi.org/10.1016/j.geomorph.2019.03.023>
- Matsuoka, N. & Murton, J. (2008) Frost weathering: recent advances and future directions. *Permafrost and Periglacial Processes*, 19(2), 195–210. Available from: <https://doi.org/10.1002/ppp.620>
- Matsuoka, N. & Sakai, H. (1999) Rockfall activity from an alpine cliff during thawing periods. *Geomorphology*, 28(3–4), 309–328. Available from: [https://doi.org/10.1016/S0169-555X\(98\)00116-0](https://doi.org/10.1016/S0169-555X(98)00116-0)
- Mayer, T., Deprez, M., Schröer, L., Cnudde, V. & Draebing, D. (2023a) Quantifying frost weathering induced rock damage in high alpine rockwalls. In: *The cryosphere discussions, September*. Göttingen, Allemagne: Copernicus Publications, pp. 1–26.
- Mayer, T., Eppes, M. & Draebing, D. (2023b) Influences driving and limiting the efficacy of ice segregation in Alpine rocks. *Geophysical Research Letters*, 50(13), 1–10. Available from: <https://doi.org/10.1029/2023GL102951>
- Mearns, L., McGinnis, S., Korytina, D., Arritt, R., Biner, S. & Bukovsky, M. (2017) *The NA-Cordex dataset, version 1.0*. Boulder CO: NCAR Climate Data Gateway.
- Michoud, C., Derron, M., Horton, P., Jaboyedoff, M., Baillifard, F., Loye, A., et al. (2012) Rockfall hazard and risk assessments along roads at a regional scale: example in Swiss Alps. *Natural Hazards and Earth System Sciences*, 12(3), 615–629. Available from: <https://doi.org/10.5194/nhess-12-615-2012>
- Moore, J.R., Gischig, V., Katterbach, M. & Loew, S. (2011) Air circulation in deep fractures and the temperature field of an alpine rock slope. *Earth Surface Processes and Landforms*, 36(15), 1985–1996. Available from: <https://doi.org/10.1002/esp.2217>
- Mourey, J., Lacroix, P., Duviillard, P.A., Marsy, G., Marcer, M., Malet, E., et al. (2022) Multi-method monitoring of rockfall activity along the classic route up Mont Blanc (4809 m a.s.l.) to encourage adaptation by mountaineers. *Natural Hazards and Earth System Sciences*, 22(2), 445–460. Available from: <https://doi.org/10.5194/nhess-22-445-2022>
- Mourey, J., Perrin-Malterre, C. & Ravel, L. (2020) Strategies used by French Alpine guides to adapt to the effects of climate change. *Journal of Outdoor Recreation and Tourism*, 29(December 2019), 100278. Available from: <https://doi.org/10.1016/j.jort.2020.100278>
- Murton, J.B., Kuras, O., Krautblatter, M., Cane, T., Tschöfen, D., Uhlemann, S., et al. (2016a) Monitoring rock freezing and thawing by novel geoelectrical and acoustic techniques. *Journal of Geophysical Research - Earth Surface*, 121(12), 2309–2332. Available from: <https://doi.org/10.1002/2016JF003948>
- Murton, J.B., Ozouf, J.C. & Peterson, R. (2016b) Heave, settlement and fracture of chalk during physical modelling experiments with temperature cycling above and below 0°C. *Geomorphology*, 270, 71–87. Available from: <https://doi.org/10.1016/j.geomorph.2016.07.016>
- Murton, J.B., Peterson, R. & Ozouf, J.C. (2006) Bedrock fracture by ice segregation in cold regions. *Science*, 314(5802), 1127–1129. Available from: <https://doi.org/10.1126/science.1132127>
- Paranunzio, R., Laio, F., Chiarle, M., Nigrelli, G. & Guzzetti, F. (2016) Climate anomalies associated with the occurrence of rockfalls at high-elevation in the Italian Alps. *Natural Hazards and Earth System Sciences*, 16(9), 2085–2106. Available from: <https://doi.org/10.5194/nhess-16-2085-2016>
- Phillips, M., Haberkorn, A., Draebing, D., Krautblatter, M., Rhyner, H. & Kenner, R. (2016) Seasonally intermittent water flow through deep fractures in an Alpine rock ridge: Gemsstock, central Swiss Alps. *Cold Regions Science and Technology*, 125, 117–127. Available from: <https://doi.org/10.1016/j.coldregions.2016.02.010>
- Piteau, D.R. & Peckover, F.L. (1978) Engineering of Rock Slopes. In: Schuster, R.L. & Krizek, R.J. (Eds.) *Landslides, analysis and control, Transportation Research Board*, in: Special Report 176. Washington, DC: National Academy of Sciences, pp. 192–228.
- Popov, Y., Beardsmore, G., Clauser, C. & Roy, S. (2016) ISRM suggested methods for determining thermal properties of rocks from laboratory tests at atmospheric pressure. *Rock Mechanics and Rock Engineering*, 49, 4179–4207. Available from: <https://doi.org/10.1007/s00603-016-1070-5>
- Pröbstl-Haider, U., Hödl, C., Ginner, K. & Borgwardt, F. (2021) Climate change: impacts on outdoor activities in the summer and shoulder seasons. *Journal of Outdoor Recreation and Tourism*, 34(October 2020), 100344. Available from: <https://doi.org/10.1016/j.jort.2020.100344>
- Rabatel, A., Deline, P., Jaillat, S. & Ravel, L. (2008) Rock falls in high-alpine rock walls quantified by terrestrial lidar measurements: a case study in the Mont Blanc area. *Geophysical Research Letters*, 35(10), 1–5. Available from: <https://doi.org/10.1029/2008GL033424>
- Rapp, A. (1960) Recent development of mountain slopes in Kärkevagge and surroundings, northern Scandinavia. *Geografiska Annaler*, 42(2–3), 65–200. Available from: <https://doi.org/10.1080/20014422.1960.11880942>
- Ravel, L. & Deline, P. (2011) Climate influence on rockfalls in high-alpine steep rockwalls: the north side of the aiguilles de chamonix (mont blanc massif) since the end of the “little ice age”. *Holocene*, 21(2), 357–365. Available from: <https://doi.org/10.1177/0959683610374887>
- Rempel, A.W., Marshall, J.A. & Roering, J.J. (2016) Modeling relative frost weathering rates at geomorphic scales. *Earth and Planetary Science Letters*, 453, 87–95. Available from: <https://doi.org/10.1016/j.epsl.2016.08.019>
- Rode, M., Schnepfleitner, H. & Sass, O. (2016) Simulation of moisture content in alpine rockwalls during freeze–thaw events. *Earth Surface Processes and Landforms*, 41(13), 1937–1950. Available from: <https://doi.org/10.1002/esp.3961>
- Samuelsson, P., Jones, C.G., Willén, U., Ullerstig, A., Gollvik, S., Hansson, U., et al. (2011) The Rossby Centre regional climate model RCA3: model description and performance. *Tellus Series a: Dynamic Meteorology and Oceanography*, 63(1), 4–23. Available from: <https://doi.org/10.1111/j.1600-0870.2010.00478.x>
- Sass, O. (2005) Rock moisture measurements: techniques, results, and implications for weathering. *Earth Surface Processes and Landforms*, 30(3), 359–374. Available from: <https://doi.org/10.1002/esp.1214>
- Schnepfleitner, H., Rode, M. & Sass, O. (2018) Validation of simulated temperature profiles at rock walls in the eastern alps (Dachstein). *Permafrost and Periglacial Processes*, 29(1), 34–48. Available from: <https://doi.org/10.1002/ppp.1962>
- Schovanec, H.E. (2020) *Development of semi-automated lidar processing algorithms to correlate climate variables to rockfall patterns for a slope near Glendwood Springs, Colorado*. Golden, CO, USA: Colorado School of Mines.
- Selby, M. (1993) *Hillslope materials and processes*, 2nd edition. Oxford, Royaume-Uni.
- Šeparović, L., Alexandru, A., Laprise, R., Martynov, A., Sushama, L., Winger, K., et al. (2013) Present climate and climate change over North America as simulated by the fifth-generation Canadian regional climate model. *Climate Dynamics*, 41, 3167–3201. Available from: <https://doi.org/10.1007/s00382-013-1737-5>
- Sidle, R. & Ochiai, H. (2006) *Landslides: processes, prediction, and land use, water res monograph*, Vol. 18. Washington, USA: American Geophysical Union.
- Stock, G.M., Martel, S.J., Collins, B.D. & Harp, E.L. (2012) Progressive failure of sheeted rock slopes: the 2009–2010 Rhombus Wall rock falls in Yosemite Valley, California, USA. *Earth Surface Processes and Landforms*, 37(5), 546–561. Available from: <https://doi.org/10.1002/esp.3192>
- Sun, Z. & Ouchterlony, F. (1986) Fracture toughness of stripa granite cores. *International Journal of Rock Mechanics and Mining Science and Geomechanics Abstracts*, 23(6), 399–409. Available from: [https://doi.org/10.1016/0148-9062\(86\)92305-3](https://doi.org/10.1016/0148-9062(86)92305-3)
- Tsytoich, N.A. (1975) *The mechanics of frozen ground*. Fort Worth, TX: Scripta book company.
- van Veen, M., Hutchinson, D.J., Kromer, R., Lato, M. & Edwards, T. (2017) Effects of sampling interval on the frequency - magnitude relationship of rockfalls detected from terrestrial laser scanning using semi-automated methods. *Landslides*, 14(5), 1579–1592. Available from: <https://doi.org/10.1007/s10346-017-0801-3>

- van Vuuren, D.P., Edmonds, J., Kainuma, M., Riahi, K., Thomson, A., Hibbard, K., et al. (2011) The representative concentration pathways: An overview. *Climatic Change*, 109(1), 5–31. Available from: <https://doi.org/10.1007/s10584-011-0148-z>
- Walder, J.S. & Hallet, B. (1985) Theoretical model of the fracture of rock during freezing. *Bulletin of the Geological Society of America*, 96(3), 336–346. Available from: [https://doi.org/10.1130/0016-7606\(1985\)96<336:atmotf>2.0.co;2](https://doi.org/10.1130/0016-7606(1985)96<336:atmotf>2.0.co;2)
- Walder, J.S. & Hallet, B. (1986) The physical basis of frost weathering: toward a more fundamental and unified perspective. *Arctic and Alpine Research*, 18(1), 27–32. Available from: <https://doi.org/10.2307/1551211>
- Wegmann, M., Gudmundsson, G.H. & Haeberli, W. (1998) Permafrost changes in rock walls and the retreat of Alpine glaciers: a thermal modelling approach. *Permafrost and Periglacial Processes*, 9(1), 23–33.
- Wieczorek, G.F. & Jäger, S. (1996) Triggering mechanisms and depositional rates of postglacial slope-movement processes in the Yosemite Valley, California. *Geomorphology*, 15(1), 17–31. Available from: [https://doi.org/10.1016/0169-555X\(95\)00112-I](https://doi.org/10.1016/0169-555X(95)00112-I)
- Zadra, A., Caya, D., Côté, J., Dugas, B., Jones, C., Laprise, R., et al. (2008) The next Canadian regional climate model. *Physics in Canada*, 64, 74–83.

How to cite this article: Birien, T., Gauthier, F. & Meloche, F. (2024) Global warming impacts on rockfall frequency and magnitude due to changing frost distribution and frost cracking effectiveness. *Earth Surface Processes and Landforms*, 1–20. Available from: <https://doi.org/10.1002/esp.5913>